TECHNISCHE UNIVERSITÄT WIEN
Vienna | Austria

DISSERTATION

Development, test and application of DFT-based methods for low dimensional systems

by

Leila Kalantari

ORCID: 0000-0002-0521-5815

A thesis submitted for the purpose of obtaining the degree of
Doctor technicae (Dr. techn.),
under the supervision of
Ao. Univ. Prof. Dipl.-Ing. Dr. tech. Peter Blaha

in the

Institute of Materials Chemistry
Vienna University of Technology

October 2021

Abstract

The Kohn-Sham version of density functional theory (DFT) is the most common method for theoretical modeling of solids, surfaces and molecules at the quantum level. The accuracy of such a calculation depends on the chosen approximation for E_{xc}. The semilocal and hybrid functionals give very good results for many of systems. However, they are inaccurate for describing weak interactions, since London dispersion forces are not properly included in these approximations; better results can be obtained by adding the correlation term ($E_{c,disp}$) accounting for the dispersion forces to the semilocal/hybrid functional. A large number of nonlocal van der Waals (NL-vdW) functionals have been proposed during the last few years, such that it is not clear which one should be used. In the first part of this work, we explain treating van der Waals interactions in DFT. Moreover, we show which functional can be used to properly describe different systems.

DFT with semilocal xc potential approximations is a reliable method for calculating ground-state properties of solids, however it provides band gaps that are much smaller than experiment. For an accurate description of band gaps and band alignments, one can use more advanced and expensive approximations, like hybrid functionals or the many-body GW method. Another possibility is DFT+U, which can only be applied to localized electrons (e.g. $3d$). The modified Becke-Johnson (mBJ) potential is currently the most accurate semilocal functionals for band gaps at much lower computational time. However, it cannot be used for non-periodic and low-dimensional systems, because it requires an average of $\nabla\rho/\rho$ over the unit cell. We implemented the local mBJ method in WIEN2k and test it for some surfaces and interfaces. Then we use a locally averaged, but spatially varying function of $\nabla\rho/\rho$ or $\nabla\rho/\rho^{4/3}$ as an indicator whether a Hubbard U should be applied to a certain atom in DFT+U calculations for oxide surfaces. In the last part of this work, we perform DFT calculations to provide a detailed description of the geometry and catalytic sites for the adsorption of M_xO_y clusters (M = , Ni, Co, Fe and Mn, $x = 5$, and $y = 0, 1, ..., 5$) on the anatase $TiO_2(101)$ surface.

Zusammenfassung

Die Kohn-Sham-Version der Dichtefunktionaltheorie (DFT) ist die gebräuchlichste Methode zur theoretischen Modellierung von Festkörpern, Oberflächen und Molekülen auf Quantenebene. Die Genauigkeit solche Berechnungen hängt von der gewählten Näherung für E_{xc} ab. Semilokale und hybride Funktionale liefern sehr gute Ergebnisse für viele Systeme. Sie sind jedoch für die Beschreibung schwacher Wechselwirkungen zu ungenau, da die London-Dispersionskräfte in diesen Näherungen nicht korrekt berücksichtigt sind. Bessere Ergebnisse können durch Addition des Korrelationsterms ($E_{\mathrm{c,disp}}$) zum semilokalen/hybriden Funktional erreicht werden, der die Dispersionskräfte berücksichtigt. In den letzten Jahren wurde eine bestimmte Anzahl nicht-lokaler van-der-Waals (NL-vdW) -Funktionenale vorgeschlagen, so dass unklar ist, welches davon verwendet werden soll. Im ersten Teil dieser Arbeit erklären wir die Behandlung von van-der-Waals Wechselwirkungen in der DFT. Darüberhinaus zeigen wir welche Systeme mit verschieden Funktionalen behandelt werden können.

DFT mit semilokalen Austauschkorrelationspotentialannäherungen ist eine zuverlässige Methode zur Berechnung der Grundzustandseigenschaften von Festkörpern, führt jedoch zu Bandlücken, die viel kleiner sind als die experimentellen. Für eine genaue Beschreibung von Bandlücken und Bandausrichtungen können fortgeschrittenere und teurere Näherungen verwendet werden, wie z. B. Hybridfunktionale oder die Vielteilchen-GW-Methode. Eine weitere Möglichkeit stellt DFT+U dar, wobei diese Nährung nur auf lokalisierte Elektronen (z. B. $3d$) angewendet werden kann. Das modifizierte Becke-Johnson-Potential (mBJ) ist derzeit das genaueste semilokale Funktional für Bandlücken bei wesentlich geringerer Rechenzeit. Es kann jedoch nicht für nicht-periodische und niedrigdimensionale Systeme verwendet werden, da es einen Mittelwert von $\nabla\rho/\rho$ über die Einheitszelle benötigt. Wir haben die Methode "local mBJ" in WIEN2k implementiert und an einigen Oberflächen und Grenzschichten getestet. Weiters haben wir eine lokal gemittelte, aber räumlich variierende Funktion von $\nabla\rho/\rho$ oder $\nabla\rho/\rho^{4/3}$ verwendet, um festzulegen, ob ein Hubbard-U auf ein bestimmtes Atom in DFT+U-Berechnungen mit Oxidflächen angewendet werden soll.

Im letzten Teil führen wir Berechnungen zur Dichtefunktionaltheorie durch, um eine detaillierte Beschreibung der Geometrie und katalytischen Zentren für die Adsorption von M_xO_y Clustern (M = Cu, Ni, Co, Fe und Mn, $x = 5$, und $y = 0, 1, ..., 5$) auf der (101)-Oberfläche von Anatas TiO_2 zuerhalten

Declaration of Authorship

I, Leila Kalantari, declare that this thesis titled, 'Development, tests and application of DFT based methods specifically to lower dimensional systems' and the work presented in it are my own. I confirm that:

- This work was done wholly or mainly while in candidature for a research degree at this University.

- Where I have consulted the published work of others, this is always clearly attributed.

- Where I have quoted from the work of others, the source is always given. With the exception of such quotations, this thesis is entirely my own work.

- I have acknowledged all main sources of help.

- Where the thesis is based on work done by myself jointly with others, I have made clear exactly what was done by others and what I have contributed myself.

Signed:

_____

Date:

_____

Acknowledgements

Contents

v

Abbreviations

1(2,3)D	one (two,three)-dimensional
AFM	antiferromagnetic
AMF	around mean field
a.u.	atomic unit
CC	coupled cluster
CI	configuration interaction
cLDA	constrained local density approximation
cRPA	constrained random phase approximation
DCACP	dispersion corrected atom-centered potentials
DFT	density functional theory
DMFT	dynamical mean field theory
DOS	density of states
EFG	electric field gradient
FFT	fast Fourier transform
FLL	fully localized limit
FM	ferromagnetic
GGA	generalised gradient approximation
hcp	hexagonal closed-packed
LAP	local atomic potential
LAPW	linearised augmented plane wave
lmBJ	local modified Becke Johnson
LO (lo)	local orbital
LR	linear response
L(S)DA	local (spin) density approximation

NMR	**n**uclear **m**agnetic **r**esonance
mBJ	**m**odified **B**ecke **J**ohnson
MGGA/meta-GGA	**m**eta **g**eneralised **g**radient **a**pproximation
MP2	**M**øller-**P**lesset **P**erturbation theory
RDMFT	**r**educed **d**ensity **m**atrix **f**unctional **t**heory
RPA	**r**andom **p**hase **a**pproximation
SCAN	**s**trongly **c**onstrained and **a**ppropriately **n**ormed
TDDFT	**t**ime **d**ependent **DFT**
TMO	**t**ransition **m**etal **o**xide
UEG	**u**niform or (homogeneous) **e**lectron **g**as
vdW	**v**an **d**er **W**aals
WDA	**w**eighted **d**ensity **a**pproximation
XC	**ex**change and **c**orrelation

Physical constants and units used in this work

a_0	$=$	$0.529177249 \times 10^{-28}$m	Bohr radius
c	$=$	$2.997\ 924\ 58 \times 10^8$ ms^{-1}	speed of light
e	$=$	$1.6021773 \times 10^{-19}$ C	elementary charge
$\hbar$	$=$	$6.62607004 \times 10^{-34}$ m^{2}kgs^{-1}	Planck's constant
Ha (E$_h$)	$=$	$27.211386245988(53)$ eV	Hartree energy
m_e	$=$	$9.1093837015(28) \times 10^{-31}$ kg	electron rest mass
m_p	$=$	$1.67262192369(51) \times 10^{-27}$kg	proton rest mass
ϵ_0	$=$	$8.8541878128(13) \times 10^{12}$ A^{2}s^{4}kg^{-1}m^{-3}	vacuum dielectric constant

Chapter 1

Theoretical Background and Methods

1.1   Introduction

The challenge of computational solid state physics is to describe the observable, macroscopic properties of a solid based solely on the type and number of atoms in a unit cell of a crystalline material. The electronic structure is described by a many-particle wavefunction, which could be obtained in principle by solving the Schrödinger equation [1] for this many-particle problem,

$$\hat{H}\Psi = E\Psi. \tag{1.1}$$

with the following Hamiltonian:

$$
\begin{aligned}
\hat{H} &= \hat{T}_{\mathrm{n}} + \hat{T}_{\mathrm{e}} + \hat{V}_{\mathrm{ee}} + \hat{V}_{\mathrm{en}} + \hat{V}_{\mathrm{nn}} \\
&= -\frac{\hbar^2}{2}\sum_{I=1}^{M}\frac{\nabla_{R_I}^2}{M_I} - \frac{\hbar^2}{2}\sum_{i=1}^{N}\frac{\nabla_{\hat{r}_i}^2}{m_e} \\
&+ \frac{1}{4\pi\epsilon_0}\sum_{I=1}^{N-1}\sum_{j=i+1}^{N}\frac{e^2}{|\hat{\mathbf{r}}_i - \hat{\mathbf{r}}_j|} - \frac{1}{4\pi\epsilon_0}\sum_{i=1}^{N}\sum_{I=1}^{M}\frac{e^2 Z_I}{|\hat{\mathbf{r}}_i - \hat{\mathbf{R}}_I|} + \frac{1}{4\pi\epsilon_0}\sum_{I=1}^{M-1}\sum_{I=I+1}^{M}\frac{Z_I Z_J}{|\hat{\mathbf{R}}_I - \hat{\mathbf{R}}_J|},
\end{aligned}
\tag{1.2}
$$

where $\hat{T}_{\mathrm{n}}$ and $\hat{T}_{\mathrm{e}}$ are the kinetic energy operators of the nuclei and electrons, respectively. $\hat{V}_{ee}$ and $\hat{V}_{nn}$ are the electron-electron and nucleus-nucleus repulsion, and $\hat{V}_{\mathrm{en}}$ is the electron-nucleus attraction operators. Here $\hbar$ is Planck's constant, R_I and M_I are the position and mass of nucleus I, m_e is the electronic mass, r_i is the position of electron i, e is the

elementary charge, Z_I is the charge of nucleus, and ϵ_0 is the vacuum dielectric constant. To simplify the equation, atomic units will be used in which ($\hbar = m_e = e = 4\pi\epsilon_0 = 1$) so they can be omitted from the equation. In atomic units, the energy is expressed in Hartree. Except for relativistic effects this equation is exact. The first approximation is the adiabatic approximation by Born and Oppenheimer [2] which allows to separate the electronic from the nuclear motion,

$$\hat{H} = -\sum_{i=1}^{N} \frac{1}{2}\hat{\nabla}_i^2 + \sum_{i=1}^{N-1}\sum_{j=i+1}^{N} \frac{1}{|\hat{\mathbf{r}}_i - \hat{\mathbf{r}}_j|} - \sum_{i=1}^{N}\sum_{I=1}^{M} \frac{Z_I}{|\hat{\mathbf{r}}_i - \hat{\mathbf{R}}_I|} + \sum_{I=1}^{M-1}\sum_{I=I+1}^{M} \frac{Z_I Z_J}{|\hat{\mathbf{R}}_I - \hat{\mathbf{R}}_J|}. \quad (1.3)$$

However, even with this approximation, due to the huge number of degrees of freedom, this problem can neither be solved analytically nor can it be treated numerically except for a very few electron system. Despite of this problem, a lot of research was done to make electronic structure calculation possible. The approaches can be categorized into three groups.

- wavefunction-based methods (Hartree, Hartree-Fock, ...)

- electron density based methods (Density Functional Theory)

- Green's function based methods (GW)

1.2   Hartree Method

In wavefunction-based methods an approximate wavefunction consists of single-particle wavefunctions. One of the simplest approximation for a wavefunction is the Hartree method [3–5], where the wavefunction Ψ_H is a product of N non-interacting one-electron wavefunctions (orbitals) ψ_i:

$$\Psi_H(\mathbf{r}_1, \mathbf{r}_2, ..., \mathbf{r}_N) = \prod_{i=1}^{N} \psi_i(\mathbf{r}_i). \quad (1.4)$$

The total energy E_{tot}, which is the expectation value of the Hamiltonian operator given by (Eq. 1.3)

$$
\begin{aligned}
E_{\text{tot}}^{\text{H}}[\{\psi_i\}] &= \langle \Psi_{\text{H}} | \hat{H} | \Psi_{\text{H}} \rangle \\
&= \sum_{i=1}^{N} \int \psi_i^*(\mathbf{r}) \left(-\frac{1}{2}\nabla^2 + v_{\text{ext}}(\mathbf{r}) \right) \psi_i(\mathbf{r}) d^3r \\
&+ \frac{1}{2} \sum_{i=1}^{N} \sum_{j=1,j\neq i}^{N} \iint \frac{|\psi_i(\mathbf{r})|^2 |\psi_j(\mathbf{r}')|^2}{|\mathbf{r}-\mathbf{r}'|} d^3r d^3r' + V_{\text{nn}},
\end{aligned}
\tag{1.5}
$$

where $v_{\text{ext}}(\mathbf{r})$ (or $v_{\text{en}}(\mathbf{r})$) is the external potential which is generated by the nuclei:

$$
v_{\text{ext}}(\mathbf{r}) = -\sum_{I}^{M} \frac{Z_I}{|\mathbf{r}-\mathbf{R}_I|}.
\tag{1.6}
$$

Defining the Lagrange function

$$
L[\{\psi_i\}] = E_{\text{tot}}^{\text{H}}[\{\psi_i\}] - \sum_{i=1}^{N} \epsilon_i \left(\int |\psi_i(\mathbf{r})|^2 d^3r - 1 \right),
\tag{1.7}
$$

where the Lagrange multipliers ϵ_i are used in order to minimize the total energy by considering the normalization constraint:

$$
\frac{\delta L[\{\psi_i\}]}{\delta \psi_i^*(\mathbf{r})} = 0,
\tag{1.8}
$$

which give us the Hartree equations:

$$
\left(-\frac{1}{2}\nabla^2 + v_{\text{ext}}(\mathbf{r}) + \sum_{j=1,j\neq i}^{N} \int \frac{|\psi_j(\mathbf{r}')|^2}{|\mathbf{r}-\mathbf{r}'|} d^3r' \right) \psi_i(\mathbf{r}) = \epsilon_i \psi_i(\mathbf{r}).
\tag{1.9}
$$

The Lagrange multipliers ϵ_i are interpreted as orbital energies.

By defining the Hartree effective potential as:

$$
v_{\text{eff},i}^{\text{H}}(\mathbf{r}) = v_{\text{ext}}(\mathbf{r}) + v_{\text{H}}(\mathbf{r}) + v_i^{\text{SIC}}(\mathbf{r}),
\tag{1.10}
$$

where $v_{\mathrm{H}}(\mathbf{r})$ is the classical Coulomb interaction generated by the charge density $\rho(\mathbf{r}) = \sum_{i=1}^{N} |\psi_i|^2$,

$$v_{\mathrm{H}}(\mathbf{r}) = \int \frac{\rho(\mathbf{r}')}{|\mathbf{r} - \mathbf{r}'|} d^3 r' \tag{1.11}$$

and v_i^{SIC} is the self-interaction correction to the classical Hartree potential v_{H}:

$$v_i^{\mathrm{SIC}}(\mathbf{r}) = -\int \frac{|\psi_i(\mathbf{r}')|^2}{|\mathbf{r} - \mathbf{r}'|} d^3 r'. \tag{1.12}$$

The Hartree equations can be rewritten:

$$\left(-\frac{1}{2}\nabla^2 + v_{\mathrm{eff},i}^{\mathrm{H}}(\mathbf{r}) \right) \psi_i(\mathbf{r}) = \epsilon_i \psi_i(\mathbf{r}). \tag{1.13}$$

The Hartree equations are in the form of one-particle Schrödinger equations and have to be solved self-consistently.

1.3 Hartree-Fock Method

The Hartree-Fock (HF) method [6–9] is an extension of the Hartree approximation which satisfies the Pauli exclusion principle. In this method, instead of using a simple product form of the wavefunction, a Slater determinant Φ_{HF}, which is constructed from a set of orthonormal one-electron orbitals $\psi_i(\mathbf{r}_i)\chi_i(s_i)$, is used to satisfy the symmetry requirement,

$$\Phi_{\mathrm{HF}}(\mathbf{r}_1, s_1, \mathbf{r}_2, s_2, ..., \mathbf{r}_N, s_N) = \frac{1}{\sqrt{N!}} \begin{vmatrix} \psi_1(\mathbf{r}_1)\chi_1(s_1) & \psi_1(\mathbf{r}_2)\chi_1(s_2) & \cdots & \psi_1(\mathbf{r}_N)\chi_1(s_N) \\ \psi_2(\mathbf{r}_1)\chi_2(s_1) & \psi_2(\mathbf{r}_2)\chi_2(s_2) & \cdots & \psi_2(\mathbf{r}_N)\chi_2(s_N) \\ \vdots & \vdots & \ddots & \vdots \\ \psi_N(\mathbf{r}_1)\chi_N(s_1) & \psi_N(\mathbf{r}_2)\chi_N(s_2) & \cdots & \psi_N(\mathbf{r}_N)\chi_N(s_N) \end{vmatrix}. \tag{1.14}$$

With this construction, Φ_{HF} is antisymmetric under exchange of two orbitals or coordinates, which is necessary for fermionic wavefunctions. In Eq. (1.14), ψ_i is the spatial part of the

wavefunction and χ_i is the spin part, which satisfies:

$$\chi_i(s) = \delta_{s\sigma_i},$$

where σ_i is the spin of the electron and $\delta_{s\sigma_i}$ is the Kronecker symbol. The spin can take one of two states which will be denoted as $\uparrow$ and $\downarrow$, $\chi_i(s)$ can have the values 0 or 1.

$$\delta_{s\sigma_i} = \begin{cases} 1 & \text{if } (s, \sigma_i) = (\uparrow, \uparrow) \text{ or } (\downarrow, \downarrow) \\ 0 & \text{if } (s, \sigma_i) = (\uparrow, \downarrow) \text{ or } (\downarrow, \uparrow) \end{cases}$$

The total energy $E_{\text{tot}}^{\text{HF}}$ is the expectation value of the Hamiltonian, which consists of the kinetic energy of electrons, the electron-nucleus attraction, the classic electron-electron repulsion (Hartree energy), the HF exchange energy and the repulsion between nuclei, respectively:

$$
\begin{aligned}
E_{\text{tot}}^{\text{HF}}[\{\psi_i\}] &= \langle \Phi_{\text{HF}} | \hat{H} | \Phi_{\text{HF}} \rangle \\
&= \sum_{i=1}^{N} \int \psi_i^*(\mathbf{r}) \left(-\frac{1}{2}\nabla^2 + v_{\text{ext}}(\mathbf{r}) \right) \psi_i(\mathbf{r}) d^3r \\
&+ \frac{1}{2} \sum_{i=1}^{N} \sum_{j=1}^{N} \iint \frac{|\psi_i(\mathbf{r})|^2 |\psi_j(\mathbf{r}')|^2}{|\mathbf{r} - \mathbf{r}'|} d^3r d^3r' \\
&- \frac{1}{2} \sum_{i=1}^{N} \sum_{j=1}^{N} \delta_{\sigma_i \sigma_j} \iint \frac{\psi_i^*(\mathbf{r})\psi_j(\mathbf{r})\psi_j^*(\mathbf{r}')\psi_i(\mathbf{r}')}{|\mathbf{r} - \mathbf{r}'|} d^3r d^3r' + V_{\text{nn}},
\end{aligned}
\tag{1.15}
$$

the third term in this equation is the HF exchange energy:

$$E_{\text{x}}^{\text{HF}}[\{\psi_i\}] = -\frac{1}{2} \sum_{i=1}^{N} \sum_{j=1}^{N} \delta_{\sigma_i \sigma_j} \iint \frac{\psi_i^*(\mathbf{r})\psi_j(\mathbf{r})\psi_j^*(\mathbf{r}')\psi_i(\mathbf{r}')}{|\mathbf{r} - \mathbf{r}'|} d^3r d^3r'. \tag{1.16}$$

Defining the Lagrange function like in the Hartree method,

$$L[\{\psi_i\}] = E_{\text{tot}}^{\text{HF}}[\{\psi_i\}] - \sum_{i=1}^{N} \sum_{j=1}^{N} \epsilon_{ij} \left(\delta_{\sigma_i \sigma_j} \int \psi_i^*(\mathbf{r})\psi_j(\mathbf{r}) d^3r - \delta_{ij} \right), \tag{1.17}$$

where the Lagrange multipliers ϵ_{ij} are used to minimize the total energy by considering the normalization constraint. After minimizing the Eq. (1.17) with respect to wavefunction ψ_i

and unitary transformation of the matrix ϵ_{ij}, the self-consistent HF equations become,

$$\left(-\frac{1}{2}\nabla^2 + v_{\text{ext}}(\mathbf{r}) + v_{\text{H}}(\mathbf{r}) \right)\psi_i(\mathbf{r}) - \sum_{j=1}^{N} \delta_{\sigma_i \sigma_j} \psi_j(\mathbf{r}) \int \frac{\psi_j^*(\mathbf{r}')\psi_i(\mathbf{r}')}{|\mathbf{r} - \mathbf{r}'|} d^3 r' = \epsilon_i \psi_i(\mathbf{r}), \quad (1.18)$$

where v_{H} is the Hartree potential given in Eq. (1.11). By defining the Hartree-Fock effective potential as:

$$v_{\text{eff},i}^{\text{HF}}(\mathbf{r}) = v_{\text{ext}}(\mathbf{r}) + v_{\text{H}}(\mathbf{r}) + v_{\text{x},i}^{\text{HF}}(\mathbf{r}), \quad (1.19)$$

where

$$\begin{aligned} v_{\text{x},i}^{\text{HF}}(\mathbf{r}) &= -\sum_{j=1}^{N} \delta_{\sigma_i \sigma_j} \frac{\psi_j(\mathbf{r})}{\psi_i(\mathbf{r})} \int \frac{\psi_j^*(\mathbf{r}')\psi_i(\mathbf{r}')}{|\mathbf{r} - \mathbf{r}'|} d^3 r' \\ &= v_i^{\text{SIC}}(\mathbf{r}) - \sum_{j=1, j\neq i}^{N} \delta_{\sigma_i \sigma_j} \frac{\psi_j(\mathbf{r})}{\psi_i(\mathbf{r})} \int \frac{\psi_j^*(\mathbf{r}')\psi_i(\mathbf{r}')}{|\mathbf{r} - \mathbf{r}'|} d^3 r' \end{aligned} \quad (1.20)$$

is the HF exchange potential. The self-consistent Hartree-Fock equations (single-particle Schrödinger-like equation for each orbital ψ_i) can be rewritten as

$$\left(-\frac{1}{2}\nabla^2 + v_{\text{eff},i}^{\text{HF}}(\mathbf{r}) \right)\psi_i(\mathbf{r}) = \epsilon_i \psi_i(\mathbf{r}). \quad (1.21)$$

HF describes exchange correctly, but correlation is totally missing. Correlation can be included in various (expensive) methods like Møller-Plesset Perturbation theory (MP2), coupled cluster (CC) or full configuration interaction (CI).

1.4 Density Functional Theory

Introduction

Density functional theory (DFT) is a standard technique in computational chemistry and material science due to its low computational cost combined with useful accuracy. However, DFT still has many limitations: too many approximation, too slow for liquids, failures for strongly correlated system, etc.

1.4.1 The Hohenberg-Kohn Theorem

The basis of DFT are two theorems presented by Hohenberg and Kohn in 1964 [10].

Theorem I: For any system of interacting particles in an external potential $V_{\text{ext}}(\mathbf{r})$, the potential is determined uniquely only by the ground state particle density ρ_0, except for a constant. It means that every observable which can be expressed as an expectation value of an operator for Ψ_0 is determined only by the ground state density.

Proof of Theorem I

This theorem can be proven by reductio ad absurdum as follows:

We consider a Hamiltonian with $V_1(\mathbf{r}) \neq V_2(\mathbf{r})$ associated with the same ground state density $\rho(\mathbf{r})$, and the two corresponding ground state many-body wavefunctions $\Psi_1(\mathbf{r})$ and $\Psi_2(\mathbf{r})$. Decompose $\hat{H}_i = \hat{F} + V_i(\mathbf{r})$, with $\hat{F}$ describing the electron kinetic energy and $V_i(\mathbf{r})$ the electron-electron interaction. We can use the variational principle to write:

$$E_1 = \langle \Psi_1 | \hat{H} | \Psi_1 \rangle < \langle \Psi_2 | \hat{H} | \Psi_2 \rangle = E_2 + \int \rho(\mathbf{r})(V_1(\mathbf{r}) - V_2(\mathbf{r})) d^3 r, \qquad (1.22)$$

where E_1 is the ground state energy corresponding to $|\Psi_1\rangle$ and E_2 is the ground state energy corresponding to $|\Psi_2\rangle$.

With the same reasoning, one obtains:

$$E_2 = \langle \Psi_2 | \hat{H} | \Psi_2 \rangle < \langle \Psi_1 | \hat{H} | \Psi_1 \rangle = E_1 + \int \rho(\mathbf{r})(V_2(\mathbf{r}) - V_1(\mathbf{r})) d^3 r. \qquad (1.23)$$

Adding both equations yields the following contradiction:

$$E_1 + E_2 < E_2 + E_1, \qquad (1.24)$$

consequently the ground state many-body wavefunctions are the same ($\Psi_1 = \Psi_2$). Therefore it is proven that the ground state density determines the external potential in a unique way, which may differ only by an additive constant. This also proves that every observable can be determined by the electron density. Since the number of electrons N is determined by integration of the density ρ, V_{ext} and N define the Hamiltonian and thus all properties of the system. Therefore, the total energy E of the system can be written as a functional of

electron density ρ:

$$E = E(\rho). \tag{1.25}$$

Theorem II: For any particular $V_{\text{ext}}(\mathbf{r})$, the exact ground state energy of the system is the global minimum of the total-energy functional, and the density that minimizes this functional is the exact ground state density $\rho_0(\mathbf{r})$.

Proof of Theorem II

According to theorem one, the external potential $V(\mathbf{r})$ is uniquely determined by the electron density $\rho(\mathbf{r})$. Therefore, the ground-state many-body wavefunction Ψ, the solution of N electrons moving inside $V(\mathbf{r})$, is also a unique function of ρ, $(\Psi[\rho(\mathbf{r})])$. The total energy can be define as

$$E[\rho] := \langle \Psi[\rho] | \hat{H} | \Psi[\rho] \rangle, \tag{1.26}$$

and by the variational principle, for any other density ρ'

$$E[\rho'] = \langle \Psi[\rho'] | \hat{H} | \Psi[\rho'] \rangle > E[\rho]. \tag{1.27}$$

The total energy functional E_ρ is

$$E[\rho] = T[\rho] + V_{\text{ee}}[\rho] + \int v_{\text{ext}}(\mathbf{r})\rho(\mathbf{r})d^3r + V_{\text{nn}}. \tag{1.28}$$

Hohenberg and Kohn [10] specified the universal functional, independent of the external potential v_{ext}, $F[\rho]$ as:

$$F[\rho] = \langle \Psi | \hat{T}_{\text{e}} + \hat{V}_{\text{ee}} | \Phi \rangle = \langle \Psi | \hat{T}_{\text{e}} | \Phi \rangle + \langle \Psi | \hat{V}_{\text{ee}} | \Phi \rangle = T[\rho] + V_{\text{ee}}[\rho]. \tag{1.29}$$

The total energy becomes:

$$E[\rho] = F[\rho] + \int v_{\text{ext}}(\mathbf{r})\rho(\mathbf{r})d^3r + V_{\text{nn}}. \tag{1.30}$$

Applying the variational principle with ρ to the Lagrange function ($\frac{\delta L}{\delta \rho} = 0$),

$$L[\rho] = E_{\text{tot}}[\rho] - \mu(\int \rho(\mathbf{r})d^3r - N) \tag{1.31}$$

leads to the Euler-Lagrange equation of the electron density ρ:

$$\mu = \frac{\delta E[\rho]}{\delta \rho(\mathbf{r})}, \tag{1.32}$$

where the Lagrange multiplier μ is the chemical potential. This equation is an outcome of the Hohenberg-Kohn theorems and can be used to calculate the electron density ρ. Since the exact form of $T[\rho]$ and $V_{\text{ee}}[\rho]$ as a function of ρ in Eq. (1.28) are not known, and an accurate approximation for $T[\rho]$ is not available, useful calculations with Eq. (1.32) are not possible.

1.4.2   Total energy in DFT

According to the Hohenberg-Kohn theorem, it is possible to consider the total energy as a functional of ρ,

$$E_{\text{tot}} = E_{\text{tot}}[\rho]. \tag{1.33}$$

However, we do not know the exact mathematical expression of $E_{\text{tot}}[\rho]$ with no wavefunctions involved. We know only approximate expressions, an example is orbital-free DFT given by the Thomas-Fermi-Dirac [11–13] (TFD) functional:

$$\begin{aligned}
E_{\text{tot}}^{\text{TFD}}[\rho] &= \int \tau^{\text{TF}}(\mathbf{r})d^3r + \int v_{\text{ext}}(\mathbf{r})\rho(\mathbf{r})d^3r \\
&+ \frac{1}{2}\iint \frac{\rho(\mathbf{r})\rho(\mathbf{r}')}{|\mathbf{r}-\mathbf{r}'|}d^3r d^3r' - \frac{3}{4}(\frac{3}{\pi})^{1/3}\int \rho^{4/3}(\mathbf{r})d^3r + V_{\text{nn}},
\end{aligned} \tag{1.34}$$

where

$$\tau^{\text{TF}}(\mathbf{r}) = \frac{3}{10}(3\pi^2)^{2/3}\rho^{5/3}(\mathbf{r}), \tag{1.35}$$

is the Thomas-Fermi kinetic energy density. The main problem in the TFD functional is kinetic energy $T[\rho]$ which is one of the main component of the total energy according to the virial theorem ($T \approx -E_{\text{tot}}$). All proposed expressions for the kinetic energy are by far too inaccurate to be useful for real applications.

1.4.3 Kohn-Sham version of DFT

The main problems in orbital-free DFT are the crude approximations for the kinetic energy and neglecting the Pauli principle. In order to avoid to use an approximation for $T[\rho]$, Kohn and Sham [14] proposed to use a single Slater determinant Φ (like in the Hartee-Fock method), and to consider a fictitious system of non-interacting electrons with the same density as the interacting system. The exact kinetic energy for a single Slater determinant reads as:

$$T_{\text{s}} = \langle \Phi | \hat{T} | \Phi \rangle = -\frac{1}{2} \sum_{i=1}^{N} \int \psi_i^* \nabla^2 \psi_i(\mathbf{r}) d^3 r. \tag{1.36}$$

The total energy is:

$$E_{\text{tot}}^{\text{KS}} = T_{\text{s}}[\{\psi_i\}] + E_{\text{ext}}[\rho] + E_{\text{H}}[\rho] + E_{\text{xc}}[\rho] + V_{\text{nn}}, \tag{1.37}$$

where $E_{\text{xc}} = E_{\text{x}} + E_{\text{c}}$ is the exchange (x) and correlation energy (c). This is not a pure density functional and we can not calculate $\delta T_s / \delta \rho$ for the Euler equation. Instead $\delta T_s / \delta \psi_i^*$ is used. This leads to the famous single-particle Kohn-Sham equations ($\rho = \sum_{i=1}^{N} |\psi|^2$):

$$\left(-\frac{1}{2} \nabla^2 + v_{\text{ext}}(\mathbf{r}) + \int \frac{\rho(\mathbf{r}')}{|\mathbf{r} - \mathbf{r}'|} d^3 r' + v_{\text{xc}}(\mathbf{r}) \right) \psi_i(\mathbf{r}) = \epsilon_i \psi_i(\mathbf{r}), \tag{1.38}$$

where v_{xc} represent the exchange-correlation potential which can be derived from the functional derivative of the exchange-correlation energy functional E_{xc},

$$v_{\text{xc}} = \frac{\delta E_{\text{xc}}}{\delta \rho(\mathbf{r})}. \tag{1.39}$$

In the Kohn-Sham version of DFT both, exchange and correlation effects are included while in Hartree-Fock E_{c} and v_{c} are absent.

1.4.3.1 Total energy in Kohn-Sham DFT

In the Kohn-Sham DFT method, the total energy is

$$E_{\text{tot}}^{\text{KS}} = T_s[\{\psi_i\}] + E_{\text{ext}}[\rho] + E_{\text{H}}[\rho] + E_{\text{xc}}[\rho] + V_{\text{nn}}, \tag{1.40}$$

where T_s represents the kinetic energy of non-interacting electrons:

$$T_\text{s}[\{\psi_i\}] = -\frac{1}{2} \sum_{i=1}^{N} \int \psi_i^* \nabla^2 \psi_i(\mathbf{r}) d^3 r. \tag{1.41}$$

E_ext is the electron-nucleus attraction

$$E_\text{ext}[\rho] = \int v_\text{ext}(\mathbf{r}) \rho(\mathbf{r}) d^3 r, \tag{1.42}$$

where v_ext is

$$v_\text{ext}(\mathbf{r}) = -\sum_{I=1}^{M} \frac{Z_I}{|\mathbf{r} - \mathbf{R}_I|}. \tag{1.43}$$

$E_\text{H}[\rho]$ is classic electron-electron repulsion:

$$E_\text{H}[\rho] = \frac{1}{2} \int \int \frac{\rho(\mathbf{r})\rho(\mathbf{r}')}{|\mathbf{r} - \mathbf{r}'|} d^3 r d^3 r', \tag{1.44}$$

and V_nn is nucleus-nucleus repulsion:

$$V_\text{nn} = \sum_{I=1}^{M-1} \sum_{J=I+1}^{M} \frac{Z_I Z_J}{|\mathbf{R}_I - \mathbf{R}_J|}. \tag{1.45}$$

In the total energy, the exact mathematical form for all components are known except for E_xc. The exchange energy E_x comes from the Pauli exclusion principle like in Hartree-Fock, while the correlation energy E_c comes from other types of many-body quantum correlations which are totally missing in Hartree-Fock like electron-electron interaction with opposite spin. In Kohn-Sham DFT, E_xc is defined such that the total energy is exact $E_\text{tot}^\text{KS} = E_\text{tot}^\text{exact}$.

$$E_\text{xc} = E_\text{tot}^\text{exact} - (T_\text{s}[\{\psi_i\}] + E_\text{ext}[\rho] + E_\text{H}[\rho] + V_\text{nn}) \tag{1.46}$$

$$E_\text{tot}^\text{exact} = \langle \Psi^\text{exact} | \hat{H} | \Psi^\text{exact} \rangle \tag{1.47}$$

It has to be corrected for T_s versus exact T and the selfinteraction included in E_H. Since we are not able to calculate $E_\text{tot}^\text{exact}$ in general and we do not know an exact E_xc, approximation for E_xc have to be used. In the following section we will discuss about different approximations for E_xc.

1.5 Jacob's Ladder of Density Functional Theory

Introduction

DFT results depend on the accuracy of the exchange correlation energy functional $E_{\mathrm{xc}}[\rho(\mathbf{r})]$. Despite a lot of efforts to define better exchange correlation functionals, there is no systematic way known to achieve consistently a higher accuracy. The known DFT approximations are different in accuracy and computational cost and are usually categorized [15] in the so-called "Jacob's Ladder of Density Functional Theory", which is the connection between the very inaccurate Hartee method $E_{\mathrm{xc}} = 0$ and the approximation where E_{xc} is accurate enough to lead to the chemical accuracy of 1 kcal/mol, which is required to make realistic chemical predictions. This ladder has five rungs and the quality of approximation usually increases with each rung, but unfortunately the computational cost also increases.

- The functionals of the first rung depend only on the local density $\rho(\mathbf{r})$ (Local Density Approximation (LDA))

- The functionals of the second rung depend on the local density $\rho(\mathbf{r})$ and its gradient $\nabla\rho(\mathbf{r})$ (Generalized Gradient Approximation (GGA))

- The functionals of third rung depend on the local density $\rho(\mathbf{r})$, its gradient $\nabla\rho(\mathbf{r})$ and the kinetic energy density $\tau(\mathbf{r})$ (meta-GGA)

- The functionals of the fourth rung depend non-locally on the occupied orbitals $\phi^o(\mathbf{r})$ and $\phi^o(\mathbf{r}')$.

- The functionals of the fifth rung depend non-locally on the occupied and unoccupied orbitals $\phi^o(\mathbf{r})$, $\phi^o(\mathbf{r}')$, $\phi^u(\mathbf{r})$ and $\phi^u(\mathbf{r}')$.

  We should mention that in the Jacob's ladder, functionals which depend non-locally on the density $\rho(\mathbf{r})$ and $\rho(\mathbf{r}')$ are missing, like in the weighted density approximation (WDA) [16] or in van der Waals functionals [17–21]. In this chapter we discuss the various approximations and in the next chapter we will discuss van der Waals interactions.

1.5.1 The First Rung - the Local Density Approximation

In the original work of Kohn and Sham [14], they suggested that an approximation for E_{xc} depending only on the local density $\rho(\mathbf{r})$ would be sufficient to describe the exchange and correlation interaction in metals. They suggested the LDA, which is exact for the so-called uniform or (homogeneous) electron gas (UEG), which is a periodic solid where the nuclei are replaced by a positive charge that is uniformly distributed. The exchange-correlation energy for the LDA has the following simple form:

$$
\begin{aligned}
E_{\mathrm{xc}}^{\mathrm{LDA}}[\rho] &= \int \epsilon_{\mathrm{xc}}^{\mathrm{UEG}}(\rho(\mathbf{r}), \zeta(\mathbf{r}))d^3r && (1.48) \\
&= \int d^3r\big(\epsilon_{\mathrm{x}}^{\mathrm{UEG}}(\rho(\mathbf{r})) + \epsilon_{\mathrm{c}}^{\mathrm{UEG}}(\rho(\mathbf{r}), \zeta(\mathbf{r}))\big), && (1.49)
\end{aligned}
$$

where the $\epsilon_{\mathrm{xc}}^{\mathrm{UEG}}$ is the exchange-correlation energy density per volume. This energy density at $\mathbf{r}$ depends only on the local charge density $\rho(\mathbf{r})$, but surprisingly it is an appropriate way to investigate exchange and correlation contributions in realistic systems and apply it as the actual exchange-correlation functional.

Exchange: The exchange energy density for the uniform electron gas can be calculated analytically [22],

$$
\epsilon_{\mathrm{x}}^{\mathrm{UEG}} = -C_{\mathrm{x}}\rho^{4/3}, \tag{1.50}
$$

where

$$
C_{\mathrm{x}} = \frac{3}{4}\left(\frac{3}{\pi}\right)^{1/3}. \tag{1.51}
$$

Correlation: The correlation energy density of this system is obtained from numerical quasi-exact quantum Monte-Carlo simulation of the uniform electron gas for various values of ρ [23]. These results are then used for analytical fits as a function of ρ and spin-polarization ζ with a function $f(\rho, \zeta)$

$$
\epsilon_{\mathrm{c}}^{\mathrm{UEG}} = f(\rho, \zeta) \tag{1.52}
$$

where

$$
\zeta = \frac{\rho\uparrow - \rho\downarrow}{\rho}. \tag{1.53}
$$

Two accurate parametrization of the Monte Carlo data are PW92 [24] and VWN5 [25]. The LDA approximation consists of using the formulas of the UEG with the density of real system $\rho(\mathbf{r})$. The LDA approximation gives good results for some classes of solids, e.g., the 5d-transition metals [26], but it is too inaccurate for the atomization energies of molecules and solids and systematically overbind both, molecules and solids. Moreover, in semiconductors and insulators, the band gaps turn out to be too small or even absent.

1.5.2 The Second Rung - the Generalized Gradient Approximation

The first step for improvement over LDA is making use of the gradient of the density to account for the inhomogenity of the density. The simplest way of writing E_{xc} is the so-called gradient expansion approximation (GEA) [14, 27] in which E_{xc} is written as a Taylor expansion and truncating it at a higher order than LDA,

$$E_{\text{xc}}^{\text{GEA}}[\rho] = \sum_{n=0}^{\infty} E_{\text{xc},2n}[\rho] = \sum_{n=0}^{\infty} \int \epsilon_{\text{xc},2n}(\rho(\mathbf{r}), \nabla\rho(\mathbf{r}),...)d^3r. \tag{1.54}$$

However, the results obtaining from GEA are worse than LDA results. Because some conditions for the exact E_{xc}, which are fulfilled by LDA, are not obeyed by GEA. The solution for that is the GGA [28], where the energy expression Eq. (1.48) is extended by a function F_{xc} called exchange-correlation enhancement factor which depends on the electron density ρ and its derivative $\nabla\rho$, this is why GGA functionals are called 'semi-local'. The GGA functional has the following form:

$$\begin{aligned} E_{\text{xc}}^{\text{GGA}}[\rho] &= \int \epsilon_{\text{xc}}^{\text{GGA}}(\rho(\mathbf{r}), \nabla\rho(\mathbf{r}))d^3r \\ &= \int \epsilon_{\text{x}}^{\text{LDA}}(r_s(\mathbf{r}))F_{\text{xc}}(r_s(\mathbf{r}), s(\mathbf{r}))d^3r, \end{aligned} \tag{1.55}$$

where $F_{\text{xc}}(r_s, s) = F_{\text{x}}(s) + F_{\text{c}}(r_s, s)$, $r_s = [3/(4\pi\rho)]^{1/3}$ is the Wigner-Seitz radius, and s is the reduced density gradient which is dimensionless and related to $\nabla\rho$,

$$s(\mathbf{r}) = \frac{|\nabla\rho(\mathbf{r})|}{2(3\pi^2)^{1/3}\rho^{4/3}(\mathbf{r})}. \tag{1.56}$$

Many different flavours of GGAs have been proposed, but generally they can be divided into two different classes: empirical and non-empirical. The non-empirical GGAs are not fitted to experimental data and are derived directly from first principle, while the empirical GGAs may contain fitted parameters adjusted by comparison with the experimental data. In the following three different GGAs will be presented, B88 [29] as an example for an empirical one, PBE [28] as an example for a non-empirical and PBEsol [30] which is used for lattice parameters of solids and in the surface calculations in this thesis.

- B88 [29]

  The Becke-88 exchange-only functional, contains only one parameter, fits the exact Hartree-Fock exchange energies of a wide variety of free atoms. It surpassed the performance of its previous functional containing two parameters or more.

  It is known that, the exact asymptotic behavior of the exchange-energy density of any finite many-electron system is given by:

  $$\lim_{\mathbf{r}\to\infty} \epsilon_{\mathrm{x}} = -\frac{1}{\mathbf{r}}. \tag{1.57}$$

  Moreover, the asymptotic behavior of the spin density ρ_σ is also known,

  $$\lim_{r\to\infty} \rho_\sigma = e^{-a_\sigma r}. \tag{1.58}$$

  In this formula a_σ is related to the ionization potential of the system and it is a constant. The gradient-correlated exchange-energy functional that reproduces the exact asymptotic behavior of Eqs. (1.57) and (1.58) is written:

  $$E_{\mathrm{x}}^{\mathrm{B88}} = E_{\mathrm{x}}^{\mathrm{LDA}} - \beta \sum_\sigma \int \rho_\sigma^{4/3} \frac{x_\sigma^2}{(1 + 6\beta x_\sigma \mathrm{arcsinh} x_\sigma)} d^3 r, \tag{1.59}$$

  where x_σ is the dimensionless parameter,

  $$x_\sigma = \frac{|\nabla \rho_\sigma|}{\rho_\sigma^{4/3}} \tag{1.60}$$

  and β is a constant which can be easily determined by a least-squares fit to exact atomic Hatreee-Fock data. They found a best-fit value of $\beta = 0.0042$ a.u., so the

exchange-correlation enhancement factor for B88 functional is:

$$F_{\text{x}}^{\text{B88}}(s) = 1 + \frac{0.0042}{2^{1/3}C_{\text{x}}} \frac{b^2 s^2}{1 + 0.0252 bs \, \text{arcsinh}(bs)}, \tag{1.61}$$

where $b = 2(6\pi^2)^{1/3}$. The $E_{\text{x}}^{\text{B88}}$ exchange functional is also widely used in the well known hybrid functional B3LYP [31, 32] in molecular chemistry.

- PBE [28]

  Today one of the most widely used GGA-functionals for solid-state calculations is the one of Perdew, Burke, Ernzerhof (PBE), employing both the density and its gradient at each point in space. As mentioned before, PBE contains no empirical parameters, but the parameters are designed to satisfy several conditions that are known for the exact functional. Some of the conditions fulfilled by PBE are the correct homogeneous electron gas limit, it means the LDA results are recovered when the reduced density gradient is zero ($s = 0$), the Lieb-Oxford bound ($E_{\text{x}}[\rho] \geqslant E_{\text{xc}}[\rho] \geqslant -1.679 \int \rho^{4/3} d^3 r$) [33], and the LDA linear response. In PBE, the enhancement factor for exchange is a function of dimensionless density gradient (s) and two non empirical parameters (μ and κ)

  $$F_{\text{x}}^{\text{PBE}}(s) = 1 + \kappa - \frac{\kappa}{1 + \frac{\mu}{k}s^2}, \tag{1.62}$$

  where $\mu = 0.21951$ and $\kappa = 0.804$ in order to satisfy the above mentioned conditions. The correlation enhancement factor is given by

  $$F_{\text{c}}^{\text{PBE}}(s, t) = \left[1 + \frac{H^{\text{PBE}}(r_s, \zeta, t, \beta)}{\epsilon_{\text{c}}^{\text{LDA}}(r_s, \zeta)} \right], \tag{1.63}$$

  where

  $$H^{\text{PBE}}(r_s, \zeta, t) = \gamma\phi^3 \ln\left(1 + \frac{\beta}{\gamma}t^2 \frac{1 + At^2}{1 + At^2 + A^2 t^4}\right) \tag{1.64}$$

  and t is a dimensionless spin scaled density gradient

  $$t(\mathbf{r}) = \left(\frac{3\pi^2}{16}\right)^{1/3} \frac{s(\mathbf{r})}{\sqrt{r_s(\mathbf{r})}\phi(\mathbf{r})}. \tag{1.65}$$

In this equation, r_s is the Wigner-Seitz radius, ζ (Eq. 1.53) is the relative spin polarization and ϕ given by

$$\phi = \left[(1+\zeta)^{2/3} + (1-\zeta)^{2/3}\right]/2, \tag{1.66}$$

with

$$\beta = 3\mu/\pi^2 \simeq 0.066725, \tag{1.67}$$

$$\gamma = (1 - \ln 2)/\pi^2, \tag{1.68}$$

and

$$A = (\beta/\gamma)[\exp(-\epsilon_c^{\mathrm{LDA}}/(\gamma\Phi^3) - 1]^{-1}. \tag{1.69}$$

The PBE functional performs equally well for finite and infinite systems. Regarding the lattice constant of solids, there are GGA functionals which overall perform better than PBE e.g. PBEsol. However, there are classes of solids for which PBE gives the best results of all GGAs (e.g., solids containing $3d$-transition elements [34, 35])

- PBEsol [30]

  PBEsol was introduced to improve equilibrium lattice parameters of densely packed solids and their surfaces. It has the same analytical form as PBE, but in order to satisfy other conditions the values of two parameters are different. The value of μ in Eq. (1.62) was set to $\mu = \mu_{GE} = 10/81$ (which is a value from the gradient expansion) in order to satisfy the second order gradient expansion of the exchange energy, while in correlation, $\beta = 0.046$ was chosen to reproduce the accurate TPSS [36] values of the surface exchange-correlation energy of jellium. PBEsol becomes exact for solids, where real solid and their surface become truly slowly varying, and exchange dominates over correlation [37]. However, it performs badly for the thermochemistry of molecules and solids [38, 39] where a value of $\mu \approx 2\mu_{GE}$ is more appropriate [40].

1.5.3 The Third Rung: meta-GGAs

A natural development after the GGA (generalized gradient approximation), that includes only the density and its first derivative in the exchange-correlation functional, is a meta-GGA (MGGA) functional which includes the second derivative of the electron density (the Laplacian) and/or the positive kinetic energy density of the occupied Kohn-Sham orbitals. This leads to the general expression for E_{xc}:

$$E_{\text{xc}}^{\text{MGGA}} = \int \epsilon_{\text{xc}}^{\text{MGGA}}(\rho(\mathbf{r}), \nabla\rho(\mathbf{r}), \nabla^2\rho(\mathbf{r}), \tau(\mathbf{r}))d^3r, \tag{1.70}$$

where

$$\tau = (1/2)\sum_{i=1}^{N} \nabla\psi_i^*.\nabla\psi_i, \tag{1.71}$$

is the positive definite kinetic energy density. τ can be used to define a dimensionless variable (α), which can detect special regions of space that ρ and $\nabla\rho$ can not. This dimensionless variable reads as:

$$\alpha(\mathbf{r}) = \frac{\tau(\mathbf{r}) - \tau^{\text{W}}(\mathbf{r})}{\tau^{\text{TF}}(\mathbf{r})}, \tag{1.72}$$

where $\tau^{\text{TF}}(\mathbf{r})$ is the Thomas-Fermi kinetic energy density Eq. (1.35) and

$$\tau^{\text{W}}(\mathbf{r}) = \frac{1}{8}\frac{|\nabla\rho(\mathbf{r})|^2}{\rho(\mathbf{r})} \tag{1.73}$$

is the iso-orbital limit of τ (von Weizsäcker kinetic energy density).

α distinguishes covalent single ($\alpha = 0$), metallic ($\alpha \approx 1$), and weak ($\alpha >> 1$) bonds [41], similar to the "electron localization function" [$1/(1+\alpha^2)$] [42]. MGGAs are computationally efficient and can achieve high accuracy as well as order-N scaling with unit-cell size. Among many existing MGGAs, the "Strongly Constrained and Appropriately Normed Semilocal Density Funtional" (SCAN) [43] is one of the most promising one. It is nonempirical and satisfies all known possible exact constraints that a MGGA can satisfy, including some not satisfied by other well-known MGGA functionals like TPSS [36] and revTPSS [44].

1.5.4 The fourth rung: Hybrid Functionals, Treating Exchange Non-Locally

It is well known that semi-local functionals underestimate the band gap, whereas Hartree-Fock overestimates it. Therefore, a certain combination of both methods can improve the band gap. The basic idea of hybrid DFT is to treat a fraction of the exchange interaction using the Hartree-Fock method and the rest with LDA, GGA, or a MGGA. In 1993, Becke [31] proposed a form for a hybrid exchange-correlation functionals, in which the exchange energy is a linear combination of a semilocal exchange and the Hartree-Fock exchange functional, while the correlation remains purely semilocal.

$$E_{xc}^{hybrid} = \alpha_x E_x^{HF} + (1 - \alpha_x) E_x^{(M)GGA} + E_c^{(M)GGA}, \tag{1.74}$$

where

$$E_x^{HF} = -\frac{1}{2} \sum_{i=1}^{N} \sum_{j=1}^{N} \delta_{\sigma_i(i)\sigma_j(j)} \iint \psi_i^*(\mathbf{r}) \psi_j(\mathbf{r}) \nu(|\mathbf{r} - \mathbf{r}'|) \psi_j^*(\mathbf{r}') \psi_i(\mathbf{r}') d^3r d^3r' \tag{1.75}$$

with $0 \leq \alpha_x \leq 1$. For $\alpha_x = 0$ the original semilocal functional is obtained and for $\alpha_x = 1$ the HF limit is reached. In Eq. (1.75), ν is either the bare Coulomb potential $\nu = 1/|\mathbf{r} - \mathbf{r}'|$ for unscreened hybrids or a potential that is screened at long distances for screened hybrid functionals. One of the most popular hybrid functional in chemistry is the semi-imperical B3LYP (Becke, three-parameter, Lee-Yang-Parr) functional [31, 32]. Another popular hybrid functional is PBE0 [45, 46],

$$E_{xc}^{PBE0} = \frac{1}{4} E_x^{HF} + \frac{3}{4} E_x^{PBE} + E_c^{PBE} \tag{1.76}$$

where the optimal choice of α_x is 0.25. In solids, the non-locality of the exchange expression leads to a increased computational cost because dense k-meshes are required, so that it is computationally advantages to include only short ranged (screened) exchange contributions. This leads to the so called HSE hybrid functional which reads as:

$$E_{xc}^{HSE} = \frac{1}{4} E_x^{HF,SR}(\mu) + \frac{3}{4} E_x^{PBE,SR}(\mu) + E_x^{PBE,LR}(\mu) + E_c^{PBE}, \tag{1.77}$$

where LR is long range and SR denotes short range contibutions. The error function approach is used for the range seperation,

$$\frac{1}{|\mathbf{r} - \mathbf{r}'|} = \underbrace{\frac{\mathrm{erfc}(\mu|\mathbf{r} - \mathbf{r}'|)}{|\mathbf{r} - \mathbf{r}'|}}_{\mathrm{SR}} + \underbrace{\frac{1 - \mathrm{erfc}(\mu|\mathbf{r} - \mathbf{r}'|)}{|\mathbf{r} - \mathbf{r}'|}}_{\mathrm{LR}}, \tag{1.78}$$

where $\mathrm{erfc}(\mu|\mathbf{r} - \mathbf{r}'|) = 1 - \mathrm{erf}(\mu|\mathbf{r} - \mathbf{r}'|)$ is the complementary error function with a certain cut-off parameter μ. In the original HSE functional (HSE03) [47] $\mu = 0.3$ was used, while it was corrected to $\mu = 0.207$ in later work (HSE06) [47, 48]. In the WIEN2k code, the HF exchange is screened by means of the Yukawa potential [49, 50],

$$\frac{1}{|\mathbf{r} - \mathbf{r}'|} = \underbrace{\frac{e^{-\lambda|\mathbf{r}-\mathbf{r}'|}}{|\mathbf{r} - \mathbf{r}'|}}_{\mathrm{SR}} + \underbrace{\frac{1 - e^{-\lambda|\mathbf{r}-\mathbf{r}'|}}{|\mathbf{r} - \mathbf{r}'|}}_{\mathrm{LR}}, \tag{1.79}$$

where λ is the screening parameter, to eliminate the long range exchange. By scaling λ [50] one recovers more or less the HSE06 functionals.

Hybrid functionals are more accurate than LDA, GGA, MGGA for the electronic structure (band gap) of insulators, semiconductor, and the thermochemistry (atomization energy of molecules), however, because of the double integral and summations over orbitals, the calculations are much more expensive than semilocal methods. In addition, hybrid functionals are not accurate for metals and yield much too large magnetic moments for itinerant ferromagnets.

1.5.5 The Fifth Rung: Random Phase Approximation (RPA)

RPA [51–53] can be introduced into DFT via the so-called adiabatic-connection fluctuation-dissipation (ACFDT) theorem. Within this formulation, the exact exchange-correlation XC energy in Kohn-Sham DFT can be formally constructed by adiabatically switching on the Coulomb interaction between electrons, while keeping the electron density fixed at its physical value. The aim of this theorem is to find an exact expression for the E_{xc} by smoothly switching the electron-electron interaction from 0 (KS system) to 1 (fully interacting system).

From ACFDT [54, 55], an exact expression for E_{xc} reads,

$$E_{xc} = E_x^{HF}[\{\psi^{KS}\}] + E_c^{ACFDT} \tag{1.80}$$

where

$$E_c^{ACFDT} = -\int_{\lambda=0}^{1} \int d^3r \int d^3r' \frac{1}{|\mathbf{r} - \mathbf{r'}|} \int_{\omega=0}^{\infty} \frac{d\omega}{2\pi} \left\{ \chi^{\lambda}(\mathbf{r}, \mathbf{r'}, i\omega) - \chi^{KS}(\mathbf{r}, \mathbf{r'}, i\omega) \right\}. \tag{1.81}$$

In this equation, χ^{λ} is the response function of the λ interacting system and the χ^{KS} is the Kohn-Sham response function. In reciprocal space the correlation energy can be written as:

$$
\begin{aligned}
E_c^{ACFDT} &= -\int_{\lambda=0}^{1} \int_{\omega=0}^{\infty} \frac{d\omega}{2\pi} \sum_{\mathbf{q} \in BZ} \sum_{\mathbf{G}} \frac{4\pi}{|\mathbf{q} + \mathbf{G}|^2} \left\{ \chi_{\mathbf{G},\mathbf{G}}^{\lambda}(\mathbf{q}, i\omega) - \chi_{\mathbf{G},\mathbf{G}}^{KS}(\mathbf{q}, i\omega) \right\} \tag{1.82} \\
&= -\int_{\lambda=0}^{1} \int_{\omega=0}^{\infty} \frac{d\omega}{2\pi} \text{Tr} \left\{ \nu \left[\chi^{\lambda}(i\omega) - \chi^{KS}(i\omega) \right] \right\} \tag{1.83}
\end{aligned}
$$

where the trace is defined as,

$$\text{Tr}\{AB\} = \sum_{\mathbf{q} \in BZ} \sum_{\mathbf{G},\mathbf{G'}} A_{\mathbf{G},\mathbf{G'}} B_{\mathbf{G},\mathbf{G'}} \tag{1.84}$$

and the Coulomb kernel is given as,

$$\nu_{\mathbf{G},\mathbf{G'}}(\mathbf{q}) = \frac{4\pi}{|\mathbf{G} + \mathbf{q}|^2} \delta_{\mathbf{G},\mathbf{G'}}. \tag{1.85}$$

Eq. (1.81) is in principle exact, as long as one can evaluate the response function of the interacting electron system χ^{λ}. The relation between the linear response function of the interacting system χ^{λ} with the coupling strength λ and the non interacting KS response function χ^{KS} can be linked by a Dyson-like equation [56, 57].

$$
\begin{aligned}
\chi^{\lambda}(\mathbf{r}, \mathbf{r'}, i\omega) &= \chi^{KS}(\mathbf{r}, \mathbf{r'}, i\omega) \\
&+ \int d^3r_1 d^3r_2 \chi^{KS}(\mathbf{r}, \mathbf{r_1}, i\omega) \left(\frac{\lambda}{|\mathbf{r_1} - \mathbf{r_2}|} + f_{xc}^{\lambda}(\mathbf{r_1}, \mathbf{r_2}, i\omega) \right) \chi^{\lambda}(\mathbf{r_2}, \mathbf{r'}, i\omega),
\end{aligned}
$$

In the Random Phase Approximation (RPA), this f_{xc}^λ is set to 0, and the correlation energy can be rewritten as:

$$E_c^{\mathrm{RPA}} = \int_0^\infty \frac{d\omega}{2\pi} \mathrm{Tr}\{\ln[1 - \chi^{\mathrm{KS}}\nu] + \chi^{\mathrm{KS}}\nu]\}, \tag{1.86}$$

where ν indicates the Coulomb kernel. RPA provides a very good description of lattice constants for covalently, ionic, metallic, as well as van der Waals bonded systems [58].

1.6 Hubbard-Corrected DFT energy functional DFT+U

Introduction

DFT is the main computational tool to perform electronic structure calculation for systems of realistic complexity, however, it fails for strongly correlated systems. As we discussed in the previous section, most commonly used energy functionals are constructed as expansions around the homogeneous electron gas limit and fail in capturing the properties of systems whose ground state is characterized by more pronounced localization of electrons. The failure can be ascribed to the tendency of approximate XC functional to over-delocalize valence electrons and to over-stabilize metallic ground states. The over-delocalization of electrons is related to the failure of XC functional to cancel out the electronic self interaction in the Hartree term. One prototypical example of problematic systems are Mott insulators or charge transfer insulators like the $3d$ transition-metal oxides, which DFT often predict them to be metallic or to have very small band gaps [59, 60]. Methods like DFT+Dynamical Mean Field Theory (DFT+DMFT) [61–64], Reduced Density Matrix Functional Theory (RDMFT) [65, 66] or Hybrid functionals can improve significantly the description of correlated systems [67], but they are prohibitively expensive for big systems. On a practical level, the DFT+U method that introduces Hubbard-model parameters to represent on-site screened Coulomb (U) and exchange (J) interactions [68, 69] is one of the powerful and computationally cheap tools suitable for calculations of large systems. The Hubbard interaction is a short range interaction between electrons of opposite spin in the same quantum

orbital and the Hubbard parameter defined as

$$U = E(d^{n+1}) + E(d^{n-1}) - 2E(d^n), \tag{1.87}$$

is the Coulomb-energy cost to place two electrons at the same site. In this equation $E(d^n)$ is the total energy of a system for which n electrons fill the given d or f orbitals of a given atom.

1.6.1 Theoretical framework

1.6.1.1 General information

In the DFT+U method, strongly correlated electrons of a system (typically, localized d or f orbitals) are described using a Hubbard model [70–75], whereas the rest of the valence electrons are treated at the level of standard DFT. The total energy of a system can be written,

$$E_{\text{DFT}+U}[\rho(\mathbf{r})] = E_{\text{DFT}}[\rho(\mathbf{r})] + E_{\text{Hub}}\big[\{n^{i\sigma}_{mm'}\}\big] - E_{\text{dc}}\big[\{n^{i\sigma}\}\big], \tag{1.88}$$

where E_{DFT} is the approximate DFT total energy and E_{Hub} is the term that contains the Hubbard Hamiltonian to model correlated states. It is necessary to eliminate from E_{DFT}, the part of the interaction energy which is modeled by E_{Hub}. This is done by subtracting the so-called "double-counting" term E_{dc}. Unfortunately, E_{dc} is not uniquely defined. The two most popular choices for the "dc" term are the so-called "around-mean-field" (AMF) [76–79] and "fully localized limit" (FLL) corrections [68, 69, 80, 81]. The first is more appropriate for systems characterized by quasi-homogeneous distribution of electrons like metals and weakly correlated systems, while the latter is more suitable for materials whose electrons are more localized on specific orbitals. In the FLL formulation of DFT+U the energy functional can be written as,

$$E_{\text{DFT}+U}[\rho(\mathbf{r})] = E_{\text{DFT}}[\rho(\mathbf{r})] + \sum_l \left[\frac{U^l}{2} \sum_{m,\sigma \neq m',\sigma'} n^{l\sigma}_m n^{l\sigma'}_{m'} - \frac{U^l}{2} n^l(n^l - 1) \right], \tag{1.89}$$

where $n_m^{l\sigma}$ are the occupation numbers of localized orbital characterized by atomic site index l, state index m and spin σ, and $n^l = \sum_{m,\sigma} n_m^{l\sigma}$. The definition of the occupation number depends on the specific implementation of DFT+U. In many DFT codes they are computed from projection of KS orbitals onto the states of a localized basis set of choice (e.g., atomic state):

$$n_{mm'}^{l\sigma} = \sum_{k,v} f_{kv}^{\sigma} \langle \psi_{kv}^{\sigma} | \phi_{m'}^{l} \rangle \langle \phi_{m}^{l} | \psi_{kv}^{\sigma} \rangle \tag{1.90}$$

where the coefficient f_{kv}^{σ} is the occupations of the KS state (labeled by k-point, band (v), and spin indices), calculated by a Fermi-Dirac distribution of the corresponding single-particle energy eigenvalues. In Eq. (1.89), the expression of the corrective term as a function of the occupation numbers defined in Eq. (1.90) shows how the Hubbard correction operates selectively on the localized orbitals of the system (the most correlated ones) while all the other states continue to be treated at the level of the DFT functionals. The second and third terms of the Eq. (1.89) represent the Hubbard and the double-counting terms specified in Eq. (1.88). From the energy functional in Eq. (1.89) and the definition of the atomic orbital occupation given in Eq. (1.90), the Hubbard contribution to the KS potential can be obtain as

$$V_{\text{tot}}^{\sigma} = V_{\text{DFT}}^{\sigma} + \sum_{l,m} U^l \left(\frac{1}{2} - n_m^{l\sigma} \right) | \phi_m^l \rangle \langle \phi_m^l |. \tag{1.91}$$

This equation shows that the Hubbard potential is repulsive for less than half-filled orbitals ($n_m^{l\sigma} < 1/2$) and attractive in all the other cases. It is responsible for the increase in energy gap in the KS spectrum, and was one of the original purposes of LDA+U [80]. The opening of the gap in the band structure is only one particular aspect of the Hubbard correction. This correction is also necessary to capture the localization of the d states in a TiO_2 system with O vacancies [82], and to obtain a better description of the magnetic structure in correlated systems.

1.6.1.2 Rotationally invariant formulation

The formulation presented in Eq. (1.89) is not invariant under rotation of the atomic orbital basis set utilized to define the occupation numbers $n_m^{l\sigma}$. A unitary-transformation-invariant

formulation was presented in Ref. [83]. In that work E_{Hub} were given in a more general statement, taken from the HF theory. It reads as

$$
\begin{aligned}
E_{\text{Hub}}\big[\{n_{mm'}l\}\big] &= \frac{1}{2} \sum_{\{m\},\sigma,l} \big\{ \langle m, m''|V_{\text{ee}}|m', m'''\rangle n^{l\sigma}_{m,m'} n^{l-\sigma}_{m''m'''} \\
&+ (\langle m, m''|V_{\text{ee}}|m', m'''\rangle) \\
&- \langle m, m''|V_{\text{ee}}|m''', m'\rangle) \times n^{l\sigma}_{mm'} n^{l\sigma}_{m''m'''} \big\},
\end{aligned} \tag{1.92}
$$

where the four-index super matrix V_{ee} represents the electron-electron interactions of the localized states (e.g., d or f atomic states) which can be written as

$$
\langle m, m''|V_{\text{ee}}|m', m'''\rangle = \int d^3 r \int d^3 r' \psi^*_{lm}(\mathbf{r})\psi_{lm'}(\mathbf{r})\frac{1}{|\mathbf{r}-\mathbf{r}'|}\psi^*_{lm''}(\mathbf{r}')\psi_{lm'''}(\mathbf{r}') \tag{1.93}
$$

The expansion of the bare Coulomb kernel in spherical harmonics and separation of the localized states into radial and angular contribution yields:

$$
\langle m, m''|V_{\text{ee}}|m', m'''\rangle = \sum_k a_k(m, m', m'', m''')F^k \tag{1.94}
$$

where $0 \leq k \leq 2l$ (l is the angular quantum number of localized electrons). The angular factors a_k can be obtain as product of the Clebsh-Gordan Coefficients [84],

$$
a_k(m, m', m'', m''') = \frac{4\pi}{2k+1} \sum_{q=-k}^{k} \langle lm|Y_{kq}|lm'\rangle \langle lm''|Y^*_{kq}|lm'''\rangle. \tag{1.95}
$$

The F_k are the Slater integrals [85] including the radial part of the atomic wavefunctions, R_{nl}, and have the following expression:

$$
F^k = \int dr \int dr' r^2 r'^2 R^2_{nl}(\mathbf{r})\frac{r^k_<}{r^{k+1}_>}R^2_{nl}(\mathbf{r}') \tag{1.96}
$$

where $r_<$ and $r_>$ indicate the shorter and the larger radial distance of r and r', respectively. For d electrons, F^0, F^2, F^4 are required to calculate the V_{ee} matrix elements while for f electrons F^6 is also needed. With the definition of the "dc" term,

$$
E_{\text{dc}}\big[\{n^l_{mm'}\}\big] = \sum_l \left\{ \frac{U^l}{2}n^l(n^l-1) - \frac{J^l}{2}[n^{l\uparrow}(n^{l\uparrow}-1) + n^{l\downarrow}(n^{l\downarrow}-1)] \right\} \tag{1.97}
$$

as the mean-field approximation of the Hubbard correction (1.92), the effective Coulomb U and exchange J interaction can be computed. U and J for d orbitals are given by,

$$U = \frac{1}{(2l+1)^2} \sum_{m,m'} \langle m, m'|V_{ee}|m, m'\rangle = F^0,$$
(1.98)

and

$$J = \frac{1}{2l(2l+1)} \sum_{m \neq m',m'} \langle m, m'|V_{ee}|m, m'\rangle = \frac{F^2 + F^4}{14}.$$
(1.99)

The details about these equations are discussed in Ref. [86].

1.6.1.3 A simpler formulation

The rotationally invariant formulation of DFT+U is the most complete formulation, with orbital-dependent electronic interaction. However, it has two parameters U and J. In many cases a simpler expression of the Hubbard correction is adapted and implemented [69], in which U and J are replaced by $U_{\text{eff}}(U_l)$. This can be obtained only by keeping the lowest order Slater integrals (F^0) and neglecting all the higher order ones ($F^2 = F^4 = J = 0$). It means $a_0(m, m', m'', m''') = \delta_{m,m'}\delta_{m'',m'''}$, so (Eq. 1.89 and Eq. (1.97) can be simplified as,

$$
\begin{aligned}
E_U\big[\big\{n_{mm'}^{l\sigma}\big\}\big] &= E_{\text{Hub}}\big[\big\{n_{mm'}^l\big\}\big] - E_{\text{dc}}\big[\big\{n^l\big\}\big] \\
&= \sum_l \frac{U^l}{2}\Big[(n^l)^2 - \sum_\sigma \text{Tr}\big[(n^{l\sigma})^2\big]\Big] \\
&\quad - \sum_l \frac{U^l}{2}n^l(n^l - 1) \\
&= \sum_{l,\sigma} \frac{U^l}{2}\text{Tr}[n^{l\sigma}(1 - n^{l\sigma})].
\end{aligned}
$$
(1.100)

The simplified version of E_U still preserves the rotational invariance of E_{Hub} and E_{dc}, by its dependence on the trace of the occupation matrices and of their product. In this simple formulation, only one interaction parameter U^l is needed to define the corrective functional. In most cases the simplified version of Hubbard correction give similar results as the fully

rotationally invariant one, however, the explicit insertion of Hund's rule coupling J is crucial to get meaningful results in some systems; for instance, to describe the ground state of systems with noncolinear magnetism[87, 88], to capture correlation effects in multi-band metals [89, 90], to study heavy-fermion systems [87, 88, 91], etc.

1.6.1.4 Determination of U

In order to achieve reasonable results with DFT+U, two important points should be considered. First, although a qualitative improvement of the results for correlated systems can be obtained by DFT+U, the results depend of course on the value of the parameters U and J. Their values are often empirically calibrated such that the result for a property (e.g., band gap or oxidation energy) matches experiment. However, they can also be obtained *ab initio* by some methods like constrained-LDA (cLDA) [92–94], constrained-RPA (cRPA) [86, 95–98], or from linear response (LR) [99, 100]. Nevertheless, there is still some ambiguity as well as freedom in the numerical implementation of these methods. For instance, localized d or f orbitals in solids usually hybridize with other valence sp orbitals, causing an entangled band structure with considerable band widths, and it is difficult to uniquely define the localized states in solids.

Second, it is not even always clear, or known in advance, if U should be applied or not. In contrast to AFM TMO where a large U value of $6-8$ eV is required, in a pure transition metal (TM) the d electrons are itinerant, i.e. only weakly correlated, and no U needs to be used in principle. However, there are of course intermediate cases, and furthermore in a given (complicated) system the degree of correlation may vary from one atom to the other even of the same type. This is the case, for instance, when a surface system consists of a TMO layer adsorbed on top of a pure metal; the degree of correlation on a TM atom is expected to decrease when going from the surface (TMO-like) deep into the bulk (pure TM-like).

1.6.1.5 Density analysis for estimating the degree of on-site correlation on transition-metal atoms in extended systems

We found that quantities depending on the electron density ρ (we call them correlation estimators) can be used to distinguish between correlated and noncorrelated $3d$ TM atoms in any kind of systems [101]: bulk solids, interfaces, and surfaces. Such a quantity could in principle be used to determine, at least qualitatively, whether or not a Hubbard U correction should be applied on a TM atom.

Correlation estimators

- $\tilde{g}(\mathbf{r})$

  Our first correlation estimator is based on

  $$g(\mathbf{r}) = \frac{|\nabla\rho(\mathbf{r})|}{\rho(\mathbf{r})},\tag{1.101}$$

  where ρ is the electron density and $\nabla\rho$ the first derivative. Then, the average of g in the whole unit cell of volume V_{cell},

  $$\bar{g} = \frac{1}{V_{\text{cell}}}\int\limits_{\text{cell}} g(\mathbf{r}')d^3r'.\tag{1.102}$$

  It was also used to define the parameter c that specifies the relative weights of the two terms in the mBJ potential [102] (see chapter 3). In Ref. [103], we discussed about the ability of $\bar{g}$ to distinguish between strongly correlated TMO and itinerant elemental TM by having clearly different values. However, since $\bar{g}$ is a constant for a particular system it can not be used as a local probe and distinguish between different atoms in the same system. Furthermore, on the technical side it is not applicable to non-periodic solids, interfaces, and systems with vacuum (low-dimensional systems), since in such systems averaging a quantity in the unit cell has no meaning.

  In Ref. [101] we used a quantity that is local (i.e., position dependent) and can provide an indication about the strength of correlation on a particular atom. Using simply

Eq. (1.101) would not really work since some (local) average (as in $\bar{g}$) is still necessary in order to have a function that is able as $\bar{g}$ to distinguish between TMO and pure TM. Finally we used the smeared local estimator first suggested in Ref. [104] and then implemented by Rauch *et al.* [105, 106]. This local correlation estimator, $\tilde{g}$, is a local average of g:

$$\tilde{g}(\mathbf{r}) = \frac{1}{(2\pi\sigma^2)^{3/2}} \int g(\mathbf{r}')e^{-\frac{|\mathbf{r}-\mathbf{r}'|^2}{2\sigma^2}}\,d^3r', \tag{1.103}$$

where the smearing parameter σ determines the size of the region (centered around $\mathbf{r}$) over which g is averaged. The expression for $\tilde{g}$ is very advantageous since it can be easily calculated by using the convolution theorem if g is expanded in plane waves. Note that in periodic bulk systems, $\tilde{g}$ becomes a constant and recovers the value of Eq. (1.102) when σ is large enough.

However, for surfaces and other systems with vacuum numerical issues with $|\nabla\rho|/\rho$ that becomes very large close to the surface region need to be solved. We followed the prescription proposed in Ref. [105], which consists of modifying Eq. (1.101) as follows:

$$g(\mathbf{r}) = \frac{1-\alpha}{\beta}\left[1 - \mathrm{erf}\left(\frac{\rho(\mathbf{r})}{\rho_{\mathrm{th}}}\right)\right] + \frac{|\nabla\rho(\mathbf{r})|}{\rho(\mathbf{r})}\mathrm{erf}\left(\frac{\rho(\mathbf{r})}{\rho_{\mathrm{th}}}\right), \tag{1.104}$$

where ρ_{th} is a threshold for very low densities. For $\rho \gg \rho_{\mathrm{th}}$, $|\nabla\rho|/\rho$ is obtained, while for $\rho \ll \rho_{\mathrm{th}}$, g becomes $(1-\alpha)/\beta$. Equation (1.104) was proposed in the framework of the local mBJ potential (see chapter 3) to cope with the aforementioned problem, but also to have the correct asymptotic behavior of the local mBJ potential in the vacuum region. Here, the goal of the damping with the function $\mathrm{erf}(\rho/\rho_{\mathrm{th}})$ is more to have a faster convergence of the plane-wave expansion of g. Although the first term in Eq. (1.104) is not necessary and could be discarded for the purpose of the present work, we decided to use the full original expression from Ref. [105].

- $\tilde{s}(\mathbf{r})$

The second correlation estimator that we consider is based on the reduced density gradient s, which is used in the enhancement factor of exchange functionals of the generalized gradient

approximation (GGA) [28]. s reads

$$s(\mathbf{r}) = \frac{|\nabla \rho(\mathbf{r})|}{2(3\pi^2)^{1/3} \rho^{4/3}(\mathbf{r})}. \tag{1.105}$$

Besides a constant factor, s differs from Eq. (1.101) by the power in the denominator that makes s dimensionless. Far from the nuclei, s goes to infinity (while g goes to a constant), but does not show the large values close to surface regions like g. Similarly to the second term in Eq. (1.104) for g, we will damp s in the vacuum:

$$s(\mathbf{r}) = \frac{|\nabla \rho(\mathbf{r})|}{2(3\pi^2)^{1/3} \rho^{4/3}(\mathbf{r})} \mathrm{erf}\left(\frac{\rho(\mathbf{r})}{\rho_{\mathrm{th}}}\right) \tag{1.106}$$

and then use it in

$$\tilde{s}(\mathbf{r}) = \frac{1}{(2\pi\sigma^2)^{3/2}} \int s(\mathbf{r}') e^{-\frac{|\mathbf{r}-\mathbf{r}'|^2}{2\sigma^2}} d^3 r' \tag{1.107}$$

to get our second correlation estimator. We have shown in Ref. [101] that the value of the correlation estimators $\tilde{g}$ and $\tilde{s}$ at the nucleus of a TM atom, which are local averages of density-dependent quantities around the corresponding atom, can be used to estimate the strength of correlation of the TM atom. In bulk solids, where we usually know from experience in which systems the TM atoms are correlated, there is a very clear difference in the values of the correlation estimators between correlated (e.g., in oxides) and noncorrelated (e.g., in pure metals) TM atoms. In more complicated systems, like at interfaces or surfaces, it may be unclear whether a certain TM atom is correlated or not, however we showed that our correlation estimators are very reliable in providing a very good hint on the correlation strength. Thus, $\tilde{g}$ or $\tilde{s}$ could be used to determine for which atoms a Hubbard U correction should be applied in a DFT+U calculation. According to the results shown in Ref. [101], we would favour $\tilde{g}$ as a more reliable estimator. However, it does not seem possible to go to a more quantitative level and to find a global relation between the estimators and a specific value of U in general, although it might be possible to relate $\tilde{g}$ or $\tilde{s}$ to specific U values in systems having several TM atoms of the same type but in different environments. The supplementary materials to this paper, which include all results for different σ and different ρ_{th} for the surfaces, are given in the Appendix.

1.7 Concluding Remarks

The methodological development and tests focused on two quantities namely:

- **Improved band gaps:** In Kohn-Sham DFT, all the complexities of the many-electron system are included in the exchange-correlation XC functional. Standard semi-local approximations to the XC functionals are quite successful in predicting many properties of solids, such as the atomic structure, phonon spectra or the qualitative band structure. Unfortunately, for an accurate description of band gaps and band alignments, it is necessary to use more advanced approximations, like non-multiplicative potentials which are outside of the KS framework. There is no unique method, which works for all cases.

  One possible improvement are Hybrid functionals (see section 1.5.4), in which a fraction of exact exchange is replaced by a fraction of the LDA or GGA exchange, which increases the band gap. However, the hybrid methods are more expensive and not satisfactory in some cases like large gap insulators. Another possibility is the LDA+U method (see section 1.6), but it can only be applied to correlated and localized electrons, e.g., $3d$ or $4f$ in transition metal and rare-earth oxides. The much more fundamental, but also much more expensive possibility is the many body GW method [107] which can be applied only to smaller systems and -as a perturbation method- in some cases depends crucially on the starting point. In 2009 Tran and Blaha [102] introduced a simple modification of the original BJ exchange potential which yields band gaps with an accuracy comparable to approaches which are orders of magnitude more expensive. The mBJ and the recently developed version of mBJ for non-periodic systems (lmBJ) will be explained in chapter 3, but as shown in Ref. [108] lmBJ is not always as accurate for 2D-systems as it is for bulk solids. The GLLB-SC [109] potential and (m)TASK [110, 111] functional provide the band gaps that are the closest to G_0W_0 for 2D-systems.

- **Treating van der Waals dispersion forces in DFT:** In general the functionals of the LDA, GGA and MGGA yield inaccurate results for van der Waals systems. This is because these functionals depends only on local quantities and thus are unable to

describe the dynamical long-range electron correlations. Therefore, the application of these approximations to systems like weakly bound dimers, molecular crystals, bio-molecules, and many other systems where dispersion forces play an important role is questionable. Thus the lack of dispersion interactions, which is defined as the attractive part of the van der Waals (vdW)-type interaction, is one of the problems in modern DFT.

Many DFT-based methods which account for dispersion are developed in recent years. We discuss these methods in chapter 2 and investigate them thoroughly.

1.8 WIEN2k code: computational details

All the calculations in this thesis were carried out within DFT, using the all-electron, WIEN2k [112, 113] code, which is based on the full potential (linearized) augmented plane-wave FP-(L)APW+lo method. The details about basis sets will not be described here, but they can be found in Refs. [114–116]. The WIEN2k package is a computer program written mainly in Fortran which performs quantum mechanical calculations on periodic solids, using periodic boundary conditions. This package allows to study many properties related to the electronic structure of a crystalline solid: optimized atomic structure, cohesive energy, electronic band structure, electron density, density of states (DOS), various types of spectra, magnetism (ferromagnetic, antiferromagnetic and non-magnetic configurations), non-collinear magnetism, Fermi surface, optical properties, electronic polarization, electric field gradients, NMR chemical and Knight shifts, and magnetic hyperfine fields. Many different exchange-correlation potentials including the LDA, various GGAs (Perdew-Wang [24, 117, 118] or PBE [119], Wu-Cohen [120]), MGGA [36, 43, 44], the DFT+U method [76] in various flavors for the double counting terms, as well as the so-called Tran-Blaha modified Becke-Johnson potential [102] and the local modified Becke-Johnson potential (lmBJ) [106], and hybrid functionals [50, 121] are implemented in this code. Aside from many semilocal functionals that are directly implemented in the WIEN2k code, all existing semilocal functionals can be used via an interface to the libxc [122, 123] library of XC functionals.

For the d-electron systems in this thesis, we have also included the strong correlation effects by means of the (GGA+U) scheme, where the correlation effects were controlled by an

effective U ($U_{eff} = U - J$), where U is the on-site Coulomb repulsion and J the on-site exchange constant. The value of U is chosen for each particular case based on the correct reproduction of experimental measurements. The parameters of our calculations are always fully converged for every particular case to the required precision.

Chapter 2

Treating van der Waals dispersion forces in DFT

2.1 Introduction

As we discussed in the first chapter, DFT is in principle exact, however in practice approximation must be made for exchange-correlation XC functionals. Many XC functionals like LDA, GGA and MGGA yield accurate results for solids. However, they fail to describe van der Waals systems, in which the cohesion is essentially due to van der Waals interactions. Thus the description of dispersion interactions which is the attractive part of the van der Waals (vdW)-type interaction, is one of the problems in modern DFT. Therefore, application of standard DFT to systems where dispersion forces are not negligible is controversial. Dispersion is an attractive interaction originating from the response of electrons in one region to instantaneous charge density fluctuations in another. This interaction leads to dipole-induced dipole interactions which decay with the well known $-1/r^6-$ behavior with inter-atomic distance r. Several DFT-based methods [17, 19, 20] which try to account for dispersion have been developed in recent years.
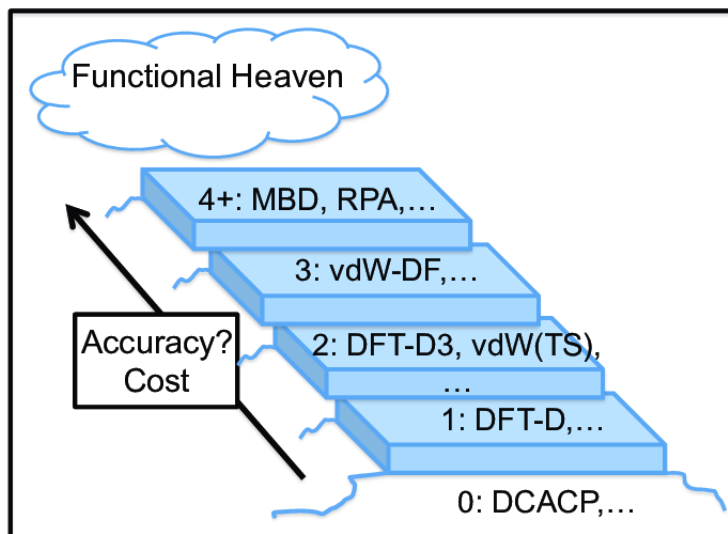
FIGURE 2.1: In analogy with Jacob's ladder classification of functional the stairway to heaven is used to classify DFT-based dispersion correction schemes [124].

2.2 Classification of the common DFT-based dispersion methods

In analogy with "Jacob's ladder" of functionals presented by Perdew [15], J. Klimeš and A. Michelides [124] introduced a "stairway to heaven" (shown in Fig 2.1) for the long range interactions and place each group of dispersion correction schemes on a different step of the stairway.

2.2.1 Ground-Step zero

At the ground level are methods, which simply do not consider the long range asymptotic. These approaches underestimate bindings of separated molecules, however, they were often used for weakly bounded systems. These are typically GGA and MGGA functionals. One exception is the LDA XC functional which was sometimes used to study graphite or noble gases on metals where the dispersion forces play a major role. However, LDA shows in most other cases the tendency to overestimate the binding. Overall, the results with the ground methods have inconsistent accuracy and the asymptotic form of interaction is incorrect.

On the ground level of the stairway, are also density functionals specifically fitted to reproduce weak interaction around the minimum. One example are the "Minnesota functionals

"[125] which are fitted to a data-set that include bindings energy of dispersion bonded dimers, amongst other properties. In pseudopotentials codes, dispersion can also be modelled by adding a specially constructed pseudpotential projector like the dispersion corrected atom-centered potentials (DCACP) [126] and the local atomic potentials (LAP) methods [127]. Although these approaches are promising [128], effort is required to fit the potentials for each element and transferability is questionable.

2.2.2 Step one (simple C_6 correction): DFT-D1/D2 methods

A basic approach to achieve the $1/r^6$ asymptotic behavior for the interaction of particles in the gas phase would be to add an additional energy term which accounts for the long-range interaction to the usual DFT energy. The total energy reads as:

$$E_{\text{tot}} = E_{\text{DFT}} + E_{\text{disp}}, \tag{2.1}$$

where the E_{DFT} is the DFT total energy and E_{disp} is the additional dispersion interaction given by

$$E_{\text{disp}} = -\sum_{A,B} C_6^{AB}/R_{AB}^6, \tag{2.2}$$

where C_6^{AB} are the dispersion coefficients which depend on the elemental pairs A and B. These methods use coefficients that are tabulated, isotropic (i.e., direction independent) and constant. Such methods are simple and computationally cheap, however they have at least four clear shortcomings:

- E_{disp} neglects both the many-body interaction and faster decaying terms like C_8/R^8 and C_{10}/R^{10} interaction.

- The C_6/R^6 function diverge for small separation.

- There is no simple ab initio way to calculate the C_6 coefficients.

- The coefficients C_6 are kept constant during the calculation, thus the effects of different chemical states of the atom and the influence of its environment are neglected.

In 2004, Grimme suggested a more consistent mean of calculating the dispersion coefficient, referred to as DFT-D1 [17]. In this method, the dispersion coefficients are obtained from a formula which couples static polarizabilities of isolated atoms and ionization potentials. The E_{disp} is an empirical dispersion correction given by

$$E_{\text{disp}} = -s_6 \sum_{A=1}^{N_{at}-1} \sum_{B=A+1}^{N_{at}} \frac{C_6^{AB}}{R_{AB}^6} f_{\text{damp}}(R_{AB}). \tag{2.3}$$

In this equation, s_6 is a global scaling factor, N_{at} is the number of atom in the system, C_6^{AB} is the dispersion coefficient for atom pair AB and R_{AB} denotes the interatomic distance. As we mentioned before, the C_6/R^6 diverges at short-atomic separations. To remedy this problem a damping function must be used which is given by

$$f_{\text{damp}}(R) = \frac{1}{1 + e^{-\alpha(R/R_0-1)}}, \tag{2.4}$$

where R_0 is the sum of atomic van der Waals radii. The damping function $f_{\text{damp}}(R_{AB}, \text{A}, \text{B})$ is equal to one for large separation and E_{disp} decreases to zero or to a constant for small separation. Different combination rules for the composed C_6^{AB} coefficients were proposed, and finally, a simple average of the following form is used in DFT-D1,

$$C_6^{AB} = 2\frac{C_6^A C_6^B}{C_6^A + C_6^B}. \tag{2.5}$$

The atomic C_6 coefficients are tabulated in Ref. [129], and have been averaged over the possible hybridization states of the atoms. The atomic C_6 coefficients are scaled by a factor s_6, which depends on the actually used density functional to account for the different behavior of the inter-molecular potential in particular at intermediate distances. In 2006, Grimme proposed a slightly different approach compared to DFT-D1, known as DFT-D2. In this approach, the scaling factor s_6 in Eq. (2.3) is different and the C_6^{AB} coefficients are obtained from the geometric mean:

$$C_6^{AB} = \sqrt{C_6^A C_6^B}. \tag{2.6}$$

The atomic C_6 is derived from the London formula for dispersion, based on DFT/PBE0

calculations of the atomic ionization potential and static dipole polarizabilities. For more details see Ref. [18]. The simple pairwise correction in step one costs zero CPU time compared to the underlying DFT calculation, so these methods are a good starting point to account for dispersion.

2.2.3 Step two (Environment-dependent C_6): DFT-D3, vdW(TS)

In "DFT-D1/D2" methods, the dispersion coefficients are predetermined and constant. Therefore, they are the same for an element regardless of its oxidation state or hybridization state.

In 2010, Grimme et al. [19, 20] presented an improved version of DFT-D methods known as DFT-D3, similar to the work of Becke and Johnson [130], and Tkatchenko and Scheffler [131, 132].

In DFT-D3, the total energy is given by

$$E_{\text{DFT-D3}} = E_{\text{DFT}} + E_{\text{disp}}, \tag{2.7}$$

where E_{DFT} is the DFT energy, and E_{disp} is the sum of two- and three-body contribution to the dispersion energy:

$$E_{\text{disp}} = E^{(2)} + E^{(3)}. \tag{2.8}$$

The most important two-body term is given by

$$E^{(2)} = -\sum_{AB} \sum_{n=6,8,10,\dots} s_n \frac{C_n^{AB}}{R_{AB}^n} f_{\text{damp},n}(R_{AB}), \tag{2.9}$$

where the first sum runs over all atom pairs in the system, C_n^{AB} is the averaged (isotropic) nth-order dispersion coefficient (n=6, 8, 10 ,...) for atom pairs AB, R_{AB} denotes their internuclear distance, and s_n is a scaling factor (DF dependent for $n > 6$) [19]. To avoid huge attractions and singularities for small distances and double counting effects of correlation at intermediate distances, the damping function $f_{\text{damp},n}$ are used.

For more information on the supported damping functions in DFT-D3, see Ref. [133]. The

dispersion coefficients are calculated *ab initio* using time dependent (TD)DFT. The starting point is the Casimir-Polder formula [134],

$$C_6^{AB} = \frac{3}{\pi} \int_0^\infty \alpha^A(i\omega)\alpha^B(i\omega)d\omega, \tag{2.10}$$

where $\alpha(i\omega)$ denotes the averaged dipole polarizability at imaginary frequency ω. The higher order of dispersion coefficient are computed recursively. They calculated dispersion coefficient for various pairs of elements in different reference (hybridization) state. In DFT-D3, the environmental dependence of the dispersion coefficients are captured by considering the number of neighbors of each atom and distances, condensed into a coordination number. The appropriate C_6 coefficient is assigned to each pair of atoms by an interpolation between the calculated reference values according to the current coordination number.

As shown in Eq. (2.8), it is possible to consider also three-body dispersion contributions with DFT-D3. Grimme et al. [19] and von Lilienfeld et al. [135] used the Axilrod-Teller-Mutto [136, 137] formula to extend the atom-centered pairwise approaches to include three-body interaction. The three-part dispersion read as:

$$E^{(3)} = -\frac{1}{6} \sum_{A \neq B \neq C} \frac{C_9^{ABC}(3\cos\theta_a \cos\theta_b \cos\theta_c + 1)}{(R_{AB}R_{BC}R_{AC})^3} f_{\text{damp}}(\overline{R}_{ABC}), \tag{2.11}$$

where θ_a, θ_b and θ_c are the internal angle of the triangle made by the A, B, and C atoms. In this formula, the dispersion coefficient C_9^{ABC} is approximated by

$$C_9^{ABC} \approx -\sqrt{C_6^{AB}C_6^{AC}C_6^{BC}}, \tag{2.12}$$

and the damping function $f_{\text{damp}}(\overline{r}_{ABC})$ is similar to Eq. (2.9). The three-body contribution has a small effect on medium-sized molecules.

Tkatchenko and Scheffler [131, 132] proposed a method, which calculated the dispersion energy according to reference atomic polarizabilites and reference atomic C_6 coefficients [138]. These quantities are enough to obtain the C_6 coefficient for a pair of different atoms [139]. Effective atomic volumes are used to obtain environment dependent dispersion coefficients. This is done by dividing the electron density of a molecule between individual atoms using the Hirshfeld partitioning scheme and for each atom its resulting density is compared to the

density of a reference state. This is used to scale the C_6 coefficient of a reference atom which changes the dispersion energy.

2.2.4 Step three: vdW-DF

In all previous methods, predetermined inputs are required to calculate dispersion interaction. Step three methods obtain the dispersion interaction directly from the electron density. These methods are called non-local correlation functionals that add non-local (i.e., long range) corrections to semi-local correlation functionals. In NL-vdW methods [21], the exchange-correlation XC functional is given by

$$E_{\text{xc}} = E_{\text{xc}}^{\text{SL/hybrid}} + E_{\text{c,disp}}^{\text{NL}}, \tag{2.13}$$

where the first term is of the semilocal (SL) or hybrid [31, 140] type, and the second term is the so-called non-local (NL) vdW dispersion of the form

$$E_{\text{c,disp}}^{\text{NL}} = \frac{1}{2} \int \int \rho(\mathbf{r}) \Phi\left(\mathbf{r}, \mathbf{r}'\right) \rho(\mathbf{r}') d^3r d^3r'. \tag{2.14}$$

In this equation, $\Phi(\mathbf{r}, \mathbf{r}')$ is an integration kernel, which is analogous to the Coulomb interaction kernel, and depends on the density ρ and its derivative $\nabla\rho$ at $\mathbf{r}$ and $\mathbf{r}'$. It can be reformulated as a function of two variables d and d',

$$\Phi(\mathbf{r}, \mathbf{r}') = \Phi(d, d'), \tag{2.15}$$

where

$$d = |\mathbf{r} - \mathbf{r}'| \, q_0(\mathbf{r}), \quad d' = |\mathbf{r} - \mathbf{r}'| \, q_0(\mathbf{r}'), \tag{2.16}$$

and

$$q_0(\mathbf{r}) = q_0(\rho(\mathbf{r}), |\nabla\rho(\mathbf{r})|). \tag{2.17}$$

The kernel $\Phi(d, d')$ has a complicated expression (see Ref. [141] and references therein). In 2004 Dion et al. [21] proposed a functional form (DRSLL) for this kernel, which could

be applied to all kind of systems. In this approach the XC energy E_{xc} is calculated by

$$E_{\text{xc}} = E_{\text{x}}^{\text{GGA}} + E_{\text{c}}^{\text{LDA}} + E_{\text{c,disp}}^{\text{NL}}, \tag{2.18}$$

which consists of the exchange energy in the revPBE [142] approximation, the LDA [24, 25] correlation energy, and the non-local correlation energy term, respectively. The double integral in Eq. (2.14) makes the calculations more expensive, but in 2009, Román-Pérez and Soler [143] proposed a very efficient method for the evaluation of Eq. (2.14) for periodic systems. This method is based on Fast Fourier Transforms (FFT) and the convolution theorem. Aside from the form of non-local (NL) vdW dispersion energy, the choice of exchange functional used in equation (2.18) is also crucial [144]. Different Kernels with different parameters according to the underlying DFT have been developed [21, 145–148]. The vdW-DF approach increase the computational time by sizeable amount compared to a GGA calculation; however, the accuracy of this approach can be higher than step one and two methods.

2.2.5 Higher steps: Random Phase Approximation (RPA)

The RPA approximation (see section 1.5.5) which provides a better description of electronic correlation energies, gives also a consistently high accuracy for solids [149], and the correct asymptotic description for the expansion of graphite, which can not be obtained by pairwise methods [150, 151]. In this step are also other methods involving orbitals like post-HF methods, MP2 coupled cluster and double hybrid functional, which are extraordinarily expensive for solids [152].

Chapter 3

Local modified Becke-Johnson exchange potential for interface, surfaces, and two-dimensional materials

3.1 Introduction

As mentioned in chapter one the electronic structure calculations of periodic solids are often performed with the Kohn-Sham (KS) method of DFT by solving the equations

$$(-\frac{1}{2}\nabla^2 + v_{\text{eff},\sigma}^{\text{KS}}(\mathbf{r}))\psi_{i,\sigma}(\mathbf{r}) = \epsilon_{i,\sigma}\psi_{i,\sigma}(\mathbf{r}), \tag{3.1}$$

where $v_{\text{eff},\sigma}^{\text{KS}} = v_{\text{ext}} + v_{\text{H}} + v_{\text{xc},\sigma}$ is the Kohn-Sham multiplicative effective potential whose components are the external, Hartree and exchange-correlation $v_{\text{xc},\sigma} = \delta E_{\text{xc}}/\delta\rho_\sigma = v_{\text{x},\sigma} + v_{\text{c},\sigma}$ potentials. In Kohn-Sham DFT all the complexities of the many-electron system are included in the exchange-correlation XC functional. Standard semi-local approximations to the XC functionals are quite successful in predicting many total-energy related ground-state properties of solids. However, they are inefficient for accurate description of band gaps and band alignments, which are excited state properties. Therefore, it is necessary to use more

sophisticated methods like the Hybrid functionals (e.g., HSE [153]) or the many-body *GW* method [107], which are very expensive. Another possibility is the LDA+*U* [76] method, but it can only be applied to correlated and localized electrons, e.g., 3*d* or 4*d* in transition and rare-earth oxides. The Becke and Johnson (BJ) [154] potential, which was designed to reproduce the shape of the optimized effective potential (OEP) (also called exact exchange method, EXX) [155, 156] improves over the LDA and PBE potential for the description of band gaps. However, the BJ potential (used in combination with LDA correlation [24]) underestimates the band gaps significantly. In 2009 Tran and Blaha [102] introduced a simple modification of the original BJ exchange potential which yields band gaps with an accuracy comparable to approaches which are orders of magnitude more expensive. In the first part of this chapter a short description of the BR, BJ and mBJ will be given. In the second part, we focus on the so-called local modified Becke-Johnson exchange potential (lmBJ) which is an another version of mBJ to obtain band structures at interfaces or systems with vacuum.

3.1.1 Becke-Roussel (BR) potential

Becke-Roussel (BR) potential [157] solves analytically the continuous exchange-hole model that satisfies all known constraints on exchange-hole functions, including non-negatively, normalization constrains and short-range behavior. It also yields exact results for both the electron gas and hydrogenic atom limits, and gives the correct $1/\mathbf{r}$ asymptotic dependence of the exchange potential in finite systems. It is completely nonempirical and yet generates energies in very good agreement with exact Hartree-Fock results in typical atomic systems. The BR potential reads

$$v_{\mathrm{x},\sigma}^{\mathrm{BR}}(\mathbf{r}) = -\frac{1}{b_\sigma(\mathbf{r})}\left(1 - e^{-x_\sigma(\mathbf{r})} - \frac{1}{2}x_\sigma(\mathbf{r})e^{-x_\sigma(\mathbf{r})}\right), \tag{3.2}$$

where x_σ is determined from a nonlinear equation involving the density, its gradient and Laplacian, and also kinetic energy density (ρ_σ, $\nabla\rho_\sigma$, $\nabla\rho_\sigma^2$ and t_σ), then b_σ is calculated with

$$b_\sigma = \left(\frac{x_\sigma^3 e^{-x_\sigma}}{8\pi\rho_\sigma}\right)^{\frac{1}{3}}. \tag{3.3}$$

Note that

$$\lim_{|\mathbf{r}|\to\infty} v_{\mathrm{x},\sigma}^{\mathrm{BR}}(\mathbf{r}) = -\frac{1}{|\mathbf{r}|},$$

(3.4)

which is the asymptotic behavior of the exact exchange potential.

3.1.2   Becke and Johnson exchange potential

In 2007, Becke and Johnson presented a simple analytical form for the exchange potential, which depends on the kinetic energy density. It was shown to reproduce well the characteristic shell structure of the exact exchange potential, obtained with the optimized effective potential method (OEP) [158] for atoms, and leads to a finite value at the position of the nuclei, which is the behavior of the exact potential [159]. It can also describe the correct $-1/\mathbf{r}$ asymptotic dependence, which is crucial in time dependent density-functional theory and in the computation of electric properties sensitive to virtual orbitals and long-range density. Calculations on solids show that the BJ exchange potential (with or without LDA/GGA correlation) leads to a better description of band gaps of semiconductors and insulators compared to the standard LDA and GGA approximations [160]. The BJ exchange potential is given by

$$v_{\mathrm{x},\sigma}^{\mathrm{BJ}}(\mathbf{r}) = v_{\mathrm{x},\sigma}^{\mathrm{BR}}(\mathbf{r}) + \frac{1}{\pi}\sqrt{\frac{5}{6}}\sqrt{\frac{\tau_\sigma(\mathbf{r})}{\rho_\sigma(\mathbf{r})}},$$

(3.5)

where

$$\tau_\sigma(\mathbf{r}) = \frac{1}{2}\sum_{i=1}^{N_\sigma} \nabla\psi_{i,\sigma}^*(\mathbf{r}).\nabla\psi_{i,\sigma}(\mathbf{r})$$

(3.6)

is the kinetic-energy density, $\rho_\sigma = \sum_{i=1}^{N_\sigma} |\psi_{i,\sigma}|^2$ is the electron density, and $v_{\mathrm{x},\sigma}^{\mathrm{BR}}(\mathbf{r})$ is the Becke-Rossel potential Eq. 3.2. Originally, Becke and Johnson used Slater potential ($v_{\mathrm{x},\sigma}^{\mathrm{Slater}}$) [9] instead of ($v_{\mathrm{x},\sigma}^{\mathrm{BR}}$), but they showed that these two potential are quasi-identical for atoms [161]. We should mention that there is no exchange-energy functional E_x whose energy functional derivative $\delta E_\mathrm{x}/\delta\rho_\sigma$ gives $v_{\mathrm{x},\sigma}^{\mathrm{BJ}}$, and therefore it can not be used to calculate total energies and geometry optimization.

3.1.3   modified Becke-Johnson exchange (mBJ) potential

The BJ exchange potential (used in combination with LDA correlation) improves over LDA and PBE for the description of band gaps for many semiconductors and insulators, however it still underestimates the band gaps significantly. In 2009 Tran and Blaha [102] presented a modified version of the semi local BJ exchange potential which was adapted to get improved band gaps. The mBJ exchange potential reads

$$v_{x,\sigma}^{mBJ}(\mathbf{r}) = c v_{x,\sigma}^{BR}(\mathbf{r}) + (3c - 2)\frac{1}{\pi}\sqrt{\frac{5}{6}}\sqrt{\frac{\tau_\sigma(\mathbf{r})}{\rho_\sigma(\mathbf{r})}}. \tag{3.7}$$

This equation is a slightly modified Eq. (3.5), where c is a system-dependent parameter and $c = 1$ corresponds to the original BJ potential. c is determined in the following empirical relation,

$$c = \alpha + \beta\left(\frac{1}{V_{cell}}\int_{cell}\frac{|\nabla\rho(r')|}{\rho(r')}d^3r'\right)^{1/2}, \tag{3.8}$$

where α and β are two free parameters which were obtained by a fit to experimental gaps, and V_{cell} is the unit cell volume. In the original work, $\alpha = -0.012$ (dimensionless) and $\beta = 1.023$ bohr$^{1/2}$ were obtained by minimization of the mean absolute relative error for the band gap of 23 solids. Other parametrizations were proposed by Koller et. al. [162] to further improve the performance of mBJ potential. Note that since $v_{x,\sigma}^{BR} \simeq v_{x,\sigma}^{Slater}$ and $v_{x,\sigma}^{BR}$ is an average of the Hartree-Fock potential [9], mBJ potential can be consider as a kind of hybrid potential whose exact exchange is given by c.

3.2   Local modified Becke-Johnson exchange potential

Although the modified Becke-Johnson MGGA exchange potential of DFT has been shown to be the best exchange potential to determine band gaps of crystalline solids, it can not be used for non-periodic systems. In the original version of TB-mBJ potential c is a material-dependent fitted parameter which is constant in the whole unit cell, that is why it cannot be consistently used to describe the electronic structure of non-periodic or nanostructured systems. In Ref. [105] Rauch et. al. proposed an effective solution to enable the use of the

mBJ potential for non-periodic systems through an inexpensive local reformulation of the parameter c. In this scheme the parameter c is substituted by a local parameter $c(\mathbf{r})$,

$$c(\mathbf{r}) = \alpha + \beta \tilde{g}(\mathbf{r})^{\epsilon}, \tag{3.9}$$

where the free parameters α, β and ϵ can be chosen from the original mBJ [102] or from the improved one [162]. In this equation $\tilde{g}(\mathbf{r})$ is a locally averaged, but spatially varying function,

$$\tilde{g}(\mathbf{r}) = \frac{1}{(2\pi\sigma^2)^{3/2}} \int g(\mathbf{r}')e^{-\frac{|\mathbf{r}-\mathbf{r}'|^2}{2\sigma^2}} d^3r', \tag{3.10}$$

that depends on a smearing parameter σ. The expression of $\tilde{g}$ is very favourable since it can be easily implemented into DFT codes using Fast-Fourier-Transforms (FFT) through the convolution of $g(\mathbf{r})$ and the Gaussian in the reciprocal space. Before using this local mBJ potential (lmBJ) for surfaces and other systems with vacuum, some issues should be solved. The correct asymptotic behavior of the XC potential $c \to 1$ in the vacuum region should be attained. Moreover, at the vacuum-matter boundary $|\nabla\rho|/\rho$ becomes very large, leading to very large XC potential and thus impede the convergence of the calculation. Another difficulty is related to vanishingly small $\rho(\mathbf{r})$ in a vacuum region, leading to numerical instabilities. All these problems can be solved by forcing $c \to 1$ for the low density region by modifying $g(\mathbf{r})$ as

$$g(\mathbf{r}) = \frac{1-\alpha}{\beta}\left[1 - \mathrm{erf}\left(\frac{\rho(\mathbf{r})}{\rho_{\mathrm{th}}}\right)\right] + \frac{|\nabla\rho(\mathbf{r})|}{\rho(\mathbf{r})}\mathrm{erf}\left(\frac{\rho(\mathbf{r})}{\rho_{\mathrm{th}}}\right), \tag{3.11}$$

where ρ_{th} is a threshold density. They chose a value corresponding to the Wigner Seitz radius $r_s^{\mathrm{th}} = (3/4\pi\rho_{\mathrm{th}})^{(1/3)} = 7$ bohr [163]. In Ref. [108, 164] we tested a variety of XC functionals as well as the lmBJ exchange potential for the calculation of the band gap of 2D materials . In Ref. [164] our test set comprises 298 2D materials for which G_0W_0 band gaps are available and were used as reference. The tested XC functionals are the most accurate currently available for band gaps. The results show that the two most accurate are the GLLB-SC potential and the mTASK functional. The lmBJ($\beta = 0.6$) potential and TASK functional can also be considered as accurate and follow quite closely GLLB-SC and mTASK.

Chapter 4

Summary of published journal articles

4.1 Computational Study of Y NMR Shielding in Intermetallic Yttrium Compounds

Leila Kalantari, Khoong Hong Khoo, Robert Laskowski, Peter Blaha; The Journal of Physical Chemistry C 121 (51), 28454-28461, 2017.

Abstract:

Density functional theory (DFT) calculations of the magnetic shielding for solid state nuclear magnetic resonance (NMR) provide an important contribution for the understanding of experimentally observed signals. In this work, we present calculations of the Y NMR shielding in intermetallic compounds. (YMg, YT, YTX, YT_2X, YT_2X_2, Y_2TB_6 and Y_2TSi_3 where T represents various transition metals and X refers to group IV elements C, Si, Ge, Sn, Pb). The total shielding σ of this selection varies by about 2500 ppm and correlates very well with the experimentally observed shifts except for YMg and YZn. These two simple compounds have a spike in the DOS at E_F and a corresponding huge spin susceptibility which leads to the disagreement. It could be a problem of DFT (neglect of spin fluctuations), but we would interpret the discrepancies as caused by disorder which could be present in the experimental samples, because disorder removes the spike in the DOS. The diamagnetic contribution σ_o (chemical shift) is by no means constant as often assumed when interpreting experimental metallic shifts and varies up to 1500 ppm, but still the dominating term is

the spin contact term σ_c. Although all compounds are metals, only half of them have a paramagnetic (negative) σ_c due to the reoccupation of the valence Y-5s electrons, while for others the large induced Y-4d magnetic moment induces a diamagnetic core polarization. In most of our cases, the spin dipolar contribution σ_{sd} is fairly small with $|\sigma_{sd}|$ less than 100 ppm, and often even much smaller except in a few very asymmetric compounds like YCo_2Si_2 and YRu_2Si_2 ($\sigma_{sd} \approx 320$ ppm).

4.2 Orbital-free approximations to the kinetic-energy density in exchange-correlation MGGA functionals: Tests on solids

Fabien Tran, Péter Kovács, Leila Kalantari, Georg K. H. Madsen, Peter Blaha; The Journal of chemical physics 149 (14), 144105, 2018.

Abstract:

A recent study of Mejia-Rodriguez and Trickey [Phys. Rev. A **96**, 052512 (2017)] showed that the deorbitalization procedure (replacing the exact Kohn-Sham kinetic-energy density by an approximate orbital-free expression) applied to exchange-correlation functionals of the meta-generalized gradient approximation (MGGA) can lead to important changes in the results for molecular properties. For the present work, the deorbitalization of MGGA functionals is further investigated by considering various properties of solids. It is shown that depending on the MGGA, common orbital-free approximations to the kinetic-energy density can be sufficiently accurate for the lattice constant, bulk modulus, and cohesive energy. For the band gap, calculated with the modified Becke-Johnson MGGA potential, the deorbitalization has a larger impact on the results.

4.3 Nonlocal van der Waals functionals for solids: Choosing an appropriate one

Fabien Tran, Leila Kalantari, Boubacar Traoré, Xavier Rocquefelte, Peter Blaha; Physical Review Materials 3 (6), 063602, 2019.

Abstract:

The nonlocal van der Waals (NL-vdW) functionals [Dion *et al.*, Phys. Rev. Lett. **92**, 246401 (2004)] are being applied more and more frequently in solid-state physics, since they have shown to be much more reliable than the traditional semilocal functionals for systems where weak interactions play a major role. However, a certain number of NL-vdW functionals have been proposed during the last few years, such that it is not always clear which one should be used. In this work, an assessment of NL-vdW functionals is presented. Our test set consists of weakly bound solids, namely rare gases, layered systems like graphite, and molecular solids, but also strongly bound solids in order to provide a more general conclusion about the accuracy of NL-vdW functionals for extended systems. We found that among the tested functionals, rev-vdW-DF2 [Hamada, Phys. Rev. B **89**, 121103(R) (2014)] is very accurate for weakly bound solids, but also quite reliable for strongly bound solids.

4.4 Semilocal exchange-correlation potentials for solid-state calculations: Current status and future directions

F Tran, J Doumont, L Kalantari, AW Huran, MAL Marques, P Blaha; Journal of Applied Physics 126 (11), 110902, 2019.

Abstract:

Kohn-Sham (KS) density functional theory (DFT) is a very efficient method for calculating various properties of solids as, for instance, the total energy, the electron density, or the electronic band structure. The KS-DFT method leads to rather fast calculations, however the accuracy depends crucially on the chosen approximation for the exchange and correlation

(xc) functional E_{xc} and/or potential v_{xc}. Here, an overview of xc methods to calculate the electronic band structure is given, with the focus on the so-called semilocal methods that are the fastest in KS-DFT and allow to treat systems containing up to thousands of atoms. Among them, there is the modified Becke-Johnson potential that is widely used to calculate the fundamental band gap of semiconductors and insulators. The accuracy for other properties like the magnetic moment or the electron density, that are also determined directly by v_{xc}, is also discussed.

4.5 Efficient Band Structure Calculation of Two-Dimensional Materials from Semilocal Density Functionals

Abstract:

The experimental and theoretical realization of 2D materials is of utmost importance in semiconducting applications. Computational modeling of these systems with satisfactory accuracy and computational efficiency is only feasible with semilocal density functional theory methods. In the search for the most useful method in predicting the band gap of 2D materials, we assess the accuracy of recently developed semilocal exchange-correlation energy functionals and potentials. Though the explicit forms of exchange-correlation(XC) potentials are very effective against XC energy functionals for the band gap of bulk solids, their performance needs to be investigated for 2D materials. In particular, the LMBJ [*J. Chem. Theory Comput.* **2020**, *16*, 2654] and GLLB-SC [*Phys. Rev. B.* **2010**, *82*, 115106] potentials are considered for their dominance in bulk band gap calculation. The performance of recently developed meta generalized gradient approximations, like TASK [*Phys. Rev. Research* **2019**, *1*, 033082] and MGGAC [*Phys. Rev. B* **2019**, *100*, 155140], is also assessed. We find that the LMBJ potential constructed for 2D materials is not as successful as its parent functional, i.e., MBJ [*Phys. Rev. Lett.* **2009**, *102*, 226401] in bulk solids. Due to a contribution from the derivative discontinuity, the band gaps obtained with GLLB-SC

are in a certain number of cases, albeit not systematically, larger than those obtained with other methods, which leads to better agreement with the quasiparticle band gap obtained from the *GW* method. The band gaps obtained with TASK and MGGAC can also be quite accurate.

4.6 Band gap of two-dimensional materials: thorough assessment of modern exchange-correlation functionals

Fabien Tran, Jan Doumont, Leila Kalantari, Peter Blaha, Tomáš Rauch, Pedro Borlido, Silvana Botti, Miguel A. L. Marques, Abhilash Patra, Subrata Jana, Prasanjit Samal; J. Chem. Phys. 155, 104103, 2021.

Abstract:

The density functional theory (DFT) approximations that are the most accurate for the calculation of band gap of bulk materials are hybrid functionals like HSE06, the MBJ potential, and the GLLB-SC potential. More recently, generalized gradient approximations (GGA), like HLE16, or meta-GGAs, like (m)TASK, have proven to be also quite accurate for the band gap. Here, the focus is on 2D materials and the goal is to provide a broad overview of the performance of DFT functionals by considering a large test set of 298 2D systems. The present work is an extension of our recent studies [Rauch *et al.*, Phys. Rev. B **101**, 245163 (2020) and Patra *et al.*, J. Phys. Chem. C **125**, 11206 (2021)]. Due to the lack of experimental results for the band gap of 2D systems, G_0W_0 results were taken as reference. It is shown that the GLLB-SC potential and mTASK functional provide the band gaps that are the closest to G_0W_0. Following closely, the local MBJ potential has a pretty good accuracy that is similar to the accuracy of the more expensive hybrid functional HSE06.

4.7 Elucidating the formation and active state of Cu co-catalysts for photocatalytic hydrogen evolution

Jasmin S. Schubert, Leila Kalantari, Andreas Lechner, Ariane Giesriegl, Sreejith P. Nandan, Pablo Alaya Leiva, Peter Blaha, Alexey Cherevan, Dominik Eder; J. Mater. Chem. A, 9(38), 21958-21971, 2021.

Abstract:

The designing of active and selective co-catalysts constitutes one of the major challenges in developing heterogeneous photocatalysts for energy conversion applications. This work provides a comprehensive insight into thermally induced bottom-up generation and transformation of a series of promising Cu-based co-catalysts. We demonstrate that the volcano-type HER profile as a function of calcination temperature is independent of the type of the Cu precursor but is affected by changes in oxidation state and location of the copper species. Supported by DFT modeling, our data suggest that low temperature ($< 200°C$) treatments facilitate electronic communication between the Cu species and TiO_2, which allows for a more efficient charge utilization and maximum HER rates. In contrast, higher temperatures ($> 200°C$) do not affect Cu oxidation state, but induce a gradual, temperature-dependent surface-to-bulk diffusion of Cu, which results in interstitial, tetra-coordinated Cu^+ species. The disappearance of Cu from the surface and the introduction of new defect states is associated with a drop in HER performance. This work examines electronic and structural effects that are in control of the photocatalytic activity and can be transferred to other systems for further advancing photocatalysis.

4.8 Density analysis for estimating the degree of on-site correlation on transition-metal atoms in extended systems

Leila Kalantari, Fabien Tran, Peter Blaha; Phys. Rev. B 104, 155127, 2021.

Abstract:

In the context of the modified Becke-Johnson (mBJ) potential, we recently underlined that $\bar{g}$, the average of $|\nabla\rho|/\rho$ in the unit cell, has markedly different values in transition-metal oxides and pure transition metals [Tran *et al.*, J. Appl. Phys. **126**, 110902 (2019)]. However, since $\bar{g}$ is a constant it is not able to provide local information about a particular atom in the system. Furthermore, while $\bar{g}$ can be used only for periodic bulk solids, a local (i.e., position-dependent) version would allow us to consider also low-dimensional systems and interfaces. Such a local function has been proposed by Rauch *et al.* [J. Chem. Theory Comput. **16**, 2654 (2020)] for the local mBJ potential. Actually, a local version of $\bar{g}$, or of another similar quantity like the reduced density gradient $\bar{s}$, could also be used in the framework of other methods. Here, we explored the idea to use such a local function $\tilde{g}$ (or $\tilde{s}$, defined as average of g (s) around a certain region of a transition metal, to estimate the degree of correlation on a transition-metal atom. We found a large difference of our correlation estimators for noncorrelated and correlated materials proving its usefulness and reliability. Our estimators can subsequently be used to determine whether a Hubbard U on-site correction in the DFT+U method should be applied to a particular atom, even in cases where it is not clear whether a particular atom should be considered as correlated or not, like in interfaces between correlated and noncorrelated materials or oxygen covered metal surfaces. In such cases, our estimators could also be used for an interpolation of U between the correlated and noncorrelated atoms.

4.9 Density functional theory study of metal and metal-oxide nucleation and growth on the anatase TiO$_2$(101) surface

Leila Kalantari, Fabien Tran, Peter Blaha (submitted)

Abstract

Experimental studies have shown the possible production of hydrogen through photocatalytic water splitting using metal oxide (MO$_y$) nanoparticles attached to an anatase TiO$_2$

surface. In this work, we performed density functional theory calculations to provide a detailed description of the stability and geometry of M_xO_y clusters M = Cu, Ni, Co, Fe and Mn, $x = 1-5$, and $y = 0-5$) on the anatase $TiO_2(101)$ surface. It is found that unsaturated 2-fold-coordinated O-sites may serve as nucleation centers for the growth of metal clusters. The formation energy of Ni-containing clusters on the anatase surface is larger than for other M clusters. In addition, the Ni_n adsorption energy increases with cluster size n, which makes the formation of bigger Ni clusters plausible as confirmed by transition electron microscopy images. Another particularity for Ni-containing clusters is that the adsorption energy per atom gets larger when the O-content is reduced, while for other M atoms it remains almost constant or, as for Mn, even decreases. This trend is in line with experimental results. Also provided is a discussion of the oxidation states of M_5O_y clusters based on their magnetic moments and Bader charges and their possible reduction with oxygen depletion.

Chapter 5

List of publication

Chapter 6

Appendix

Density analysis for estimating the degree of on-site correlation on transition-metal atoms in extended systems

Leila Kalantari, Fabien Tran, Peter Blaha

Institute of Materials Chemistry, Vienna University of Technology, Getreidemarkt 9/165-TC, A-1060 Vienna, Austria

TABLE 6.1: Values of $\tilde{g}$ on the $3d$ TM atom in correlated and non-correlated bulk solids calculated for different σ. The magnetic state is indicated in parenthesis.

solid	σ=3.78	σ=2.78	σ=1.78	$\sigma = 1.53$	σ=1.28	σ=1.03	σ=0.78
Ti (NM)	1.08	1.08	1.23	1.43	1.80	2.38	3.08
V (NM)	1.18	1.18	1.27	1.42	1.75	2.31	3.07
Cr (AFM)	1.29	1.29	1.35	1.47	1.76	2.30	3.09
Mn (NM)	1.30	1.30	1.40	1.57	1.91	2.49	3.28
Fe (FM)	1.37	1.37	1.43	1.56	1.85	2.41	3.25
FeAl (FM)	1.10	1.10	1.23	1.41	1.77	2.39	3.22
FeNi (FM)	1.45	1.45	1.50	1.62	1.90	2.44	3.27
Fe_3Ni (FM)	1.42	1.42	1.48	1.59	1.88	2.43	3.25
Fe_2P (FM)	1.33	1.33	1.42	1.58	1.90	2.48	3.29
$FeSb_2$ (FM)	1.33	1.35	1.50	1.66	1.96	2.49	3.26
Co (FM)	1.46	1.46	1.51	1.62	1.89	2.45	3.30
Ni (FM)	1.52	1.52	1.57	1.67	1.95	2.50	3.37
Cu (NM)	1.51	1.51	1.58	1.71	2.01	2.60	3.48
Cu_2Sb (NM)	1.41	1.42	1.52	1.67	2.00	2.62	3.50
Cu_3P (NM)	1.40	1.40	1.56	1.75	2.11	2.71	3.55
CuAu (NM)	1.56	1.56	1.61	1.75	2.06	2.65	3.51
Cu_3Au (NM)	1.58	1.57	1.62	1.77	2.09	2.69	3.55
Zn (NM)	1.36	1.36	1.47	1.66	2.03	2.68	3.60
TiO_2(Anatase) (NM)	1.85	1.87	2.02	2.12	2.29	2.60	3.12
TiO_2(Rutile) (NM)	1.83	1.84	1.98	2.09	2.28	2.60	3.12
Ti_2O_3 (NM)	1.77	1.78	1.90	2.01	2.21	2.56	3.10
V_2O_3 (AFM)	1.79	1.79	1.93	2.05	2.27	2.64	3.21
$SrVO_3$ (NM)	1.77	1.78	1.90	2.01	2.20	2.54	3.11
Cr_2O_3 (AFM)	1.84	1.85	1.97	2.08	2.29	2.67	3.26
CrO_2 (FM)	1.87	1.87	2.00	2.12	2.31	2.65	3.22
MnO (AFM)	1.74	1.74	1.85	2.00	2.29	2.77	3.43
MnO_2 (AFM)	1.88	1.89	2.02	2.13	2.33	2.69	3.24
Mn_2O_3 (AFM)	1.83	1.85	1.99	2.11	2.34	2.74	3.35
FeO (AFM)	1.73	1.73	1.83	1.97	2.28	2.73	3.43
Fe_2O_3 (AFM)	1.83	1.83	1.96	2.10	2.34	2.76	3.42
Fe_3O_4 (FM)	1.79	1.80	1.92	2.05	2.29	2.73	3.40
FeF_2 (AFM)	1.99	2.00	2.18	2.32	2.54	2.93	3.54
CoO (AFM)	1.77	1.77	1.86	1.99	2.27	2.75	3.47
NiO (AFM)	1.81	1.81	1.90	2.03	2.29	2.77	3.51
CuO (AFM)	1.80	1.80	1.91	2.20	2.34	2.83	3.57
Cu_2O (NM)	1.64	1.64	1.79	1.97	2.31	2.84	3.57
CuI (NM)	1.50	1.53	1.79	1.98	2.30	2.83	3.58
ZnO (NM)	1.80	1.80	1.97	2.14	2.44	2.93	3.68
$YBa_2Cu_3O_6$(FM)-Cu1,Cu2	1.58,1.72	1.56,1.74	1.81,1.89	2.03,2.05	2.37,2.33	2.86,2.82	3.36,2.36
$YBa_2Cu_3O_7$(NM)-Cu1,Cu2	1.58,1.71	1.56,1.73	1.81,1.89	2.02,2.05	2.35,2.33	2.85,2.82	3.56,3.56

TABLE 6.2: Values of $\tilde{s}$ on the $3d$ TM atom in correlated and non-correlated bulk solids calculated for different σ. The magnetic state is indicated in parenthesis.

solid	σ=3.78	σ=2.78	σ=1.78	$\sigma = 1.53$	σ=1.28	σ=1.03	σ=0.78
Ti (NM)	0.38	0.38	0.41	0.45	0.53	0.62	0.65
V (NM)	0.38	0.38	0.39	0.42	0.48	0.57	0.62
Cr (AFM)	0.39	0.39	0.40	0.41	0.46	0.53	0.59
Mn (NM)	0.44	0.44	0.47	0.50	0.57	0.68	0.75
Fe (FM)	0.47	0.47	0.48	0.50	0.53	0.59	0.62
FeAl (FM)	0.36	0.36	0.38	0.41	0.47	0.57	0.63
FeNi (FM)	0.48	0.48	0.49	0.51	0.54	0.59	0.62
Fe$_3$Ni (FM)	0.48	0.48	0.49	0.50	0.54	0.59	0.62
Fe$_2$P (FM)	0.44	0.44	0.46	0.49	0.54	0.60	0.63
FeSb$_2$ (FM)	0.52	0.52	0.52	0.53	0.57	0.61	0.63
Co (FM)	0.48	0.48	0.49	0.51	0.54	0.60	0.64
Ni (FM)	0.48	0.48	0.49	0.50	0.54	0.60	0.65
Cu (NM)	0.48	0.48	0.49	0.51	0.56	0.63	0.67
Cu$_2$Sb (NM)	0.50	0.50	0.49	0.51	0.56	0.64	0.69
Cu$_3$P (NM)	0.48	0.49	0.54	0.57	0.63	0.69	0.72
CuAu (NM)	0.51	0.51	0.52	0.54	0.59	0.66	0.70
Cu$_3$Au (NM)	0.51	0.52	0.54	0.56	0.61	0.68	0.72
Zn (NM)	0.47	0.47	0.49	0.52	0.58	0.67	0.72
TiO$_2$(Anatase) (NM)	0.89	0.88	0.81	0.78	0.75	0.72	0.67
TiO$_2$(Rutile) (NM)	0.79	0.79	0.76	0.75	0.73	0.71	0.67
Ti$_2$O$_3$ (NM)	0.73	0.73	0.71	0.71	0.71	0.70	0.66
V$_2$O$_3$ (AFM)	0.75	0.74	0.70	0.70	0.68	0.67	0.63
SrVO$_3$ (NM)	0.73	0.72	0.68	0.67	0.66	0.66	0.64
Cr$_2$O$_3$ (AFM)	0.74	0.74	0.75	0.76	0.77	0.78	0.76
CrO$_2$ (FM)	0.75	0.75	0.72	0.69	0.67	0.65	0.61
MnO (AFM)	0.68	0.67	0.66	0.66	0.67	0.68	0.63
MnO$_2$ (AFM)	0.77	0.77	0.75	0.75	0.74	0.74	0.73
Mn$_2$O$_3$ (AFM)	0.77	0.76	0.72	0.71	0.70	0.67	0.63
FeO (AFM)	0.64	0.64	0.65	0.67	0.68	0.70	0.66
Fe$_2$O$_3$ (AFM)	0.74	0.74	0.73	0.72	0.71	0.70	0.66
Fe$_3$O$_4$ (FM)	0.73	0.72	0.70	0.71	0.73	0.76	0.77
FeF$_2$ (AFM)	0.99	0.98	0.91	0.88	0.83	0.78	0.69
CoO (AFM)	0.64	0.64	0.66	0.67	0.69	0.71	0.69
NiO (AFM)	0.64	0.65	0.66	0.67	0.70	0.72	0.71
CuO (AFM)	0.77	0.77	0.77	0.78	0.79	0.80	0.78
Cu$_2$O (NM)	0.67	0.67	0.68	0.70	0.73	0.76	0.74
CuI (NM)	0.83	0.83	0.79	0.78	0.77	0.77	0.74
ZnO (NM)	0.80	0.80	0.80	0.80	0.80	0.80	0.76
YBa$_2$Cu$_3$O$_6$(FM)-Cu1,Cu2	0.77,0.71	0.77,0.71	0.78,0.70	0.78,0.71	0.79,0.72	0.78,0.73	0.73,0.72
YBa$_2$Cu$_3$O$_7$(NM)-Cu1,Cu2	0.76,0.71	0.77,0.71	0.77,0.70	0.78,0.71	0.78,0.72	0.77,0.73	0.73,0.72

TABLE 6.3: The $\tilde{g}$ for plane Ni(111) surfaces as well as Ni(111) with full oxygen coverage for different σ and different ρ_{th}, the results for Ni and NiO are added to the table only for comparison.

solid	σ=3.78	σ=2.78	σ=1.78	$\sigma = 1.53$	σ=1.28	σ=1.03	σ=0.78
Ni	1.52	1.52	1.57	1.67	1.95	2.50	3.37
NiO	1.81	1.81	1.90	2.03	2.29	2.77	3.51
Ni (Ni@surface)-ρ_{th}=0.0007	1.52	1.57	1.69	1.82	2.10	2.62	3.43
Ni (Ni@subsurface)	1.54	1.54	1.58	1.69	1.96	2.51	3.37
Ni (Ni@middle)	1.52	1.52	1.57	1.68	1.96	2.51	3.38
Ni (Ni@surface)-ρ_{th}=0.002	1.50	1.56	1.69	1.82	2.09	2.62	3.43
Ni (Ni@subsurface)	1.54	1.54	1.58	1.68	1.95	2.51	3.37
Ni (Ni@middle)	1.52	1.52	1.57	1.68	1.95	2.51	3.37
Ni (Ni@surface-ρ_{th}=0.01	1.47	1.53	1.67	1.81	2.09	2.62	3.43
Ni (Ni@subsurface)	1.53	1.54	1.58	1.69	1.96	2.50	3.37
Ni (Ni@middle)	1.52	1.52	1.57	1.68	1.96	2.51	3.39
Ni (Ni@surface)-ρ_{th}=0.015	1.46	1.52	1.67	1.80	2.08	2.62	3.43
Ni (Ni@subsurface)	1.53	1.54	1.58	1.69	1.96	2.51	3.37
Ni (Ni@middle)	1.52	1.52	1.57	1.68	1.96	2.51	3.38
Ni-full coverage (Ni@surface-ρ_{th}=0.0007	1.72	1.77	1.82	1.90	2.12	2.59	3.37
Ni-full coverage (Ni@subsurface)	1.60	1.56	1.58	1.69	1.96	2.52	3.36
Ni-full coverage (Ni@middle)	1.54	1.54	1.59	1.70	1.97	2.52	3.38
Ni-full coverage (Ni@surface)-ρ_{th}=0.002	1.70	1.75	1.81	1.90	2.11	2.58	3.36
Ni-full coverage (Ni@subsurface)	1.59	1.56	1.58	1.70	1.96	2.51	3.36
Ni-full coverage (Ni@middle)	1.54	1.54	1.59	1.70	1.97	2.52	3.37
Ni-full coverage (Ni@surface)-ρ_{th}=0.01	1.66	1.72	1.80	1.90	2.12	2.59	3.37
Ni-full coverage (Ni@subsurface)	1.58	1.56	1.58	1.69	1.96	2.52	3.36
Ni-full coverage (Ni@middle)	1.54	1.54	1.59	1.70	1.97	2.52	3.38
Ni-full coverage (Ni@surface-ρ_{th}=0.015	1.64	1.71	1.80	1.89	2.12	2.59	3.37
Ni-full coverage (Ni@subsurface	1.58	1.56	1.58	1.69	1.94	2.52	3.36
Ni-full coverage (Ni@middle)	1.53	1.54	1.59	1.70	1.97	2.52	3.38

TABLE 6.4: The $\tilde{s}$ for plane Ni(111) surfaces as well as Ni(111) with full oxygen coverage for different σ and different ρ_{th} , the results for Ni and NiO are added to the table only for comparison.

solid	σ=3.78	σ=2.78	σ=1.78	$\sigma = 1.53$	σ=1.28	σ=1.03	σ=0.78
Ni	0.48	0.48	0.49	0.50	0.54	0.60	0.65
NiO	0.64	0.65	0.66	0.67	0.70	0.72	0.71
Ni (Ni@surface)-ρ_{th}=0.004	0.57	0.61	0.63	0.63	0.64	0.67	0.68
Ni (Ni@subsurface)	0.52	0.50	0.49	0.51	0.54	0.61	0.66
Ni (Ni@middle)	0.48	0.48	0.49	0.50	0.54	0.61	0.66
Ni (Ni@surface)-ρ_{th}=0.01	0.49	0.54	0.58	0.60	0.63	0.67	0.68
Ni (Ni@subsurface)	0.50	0.50	0.49	0.51	0.54	0.61	0.66
Ni (Ni@middle)	0.48	0.48	0.49	0.50	0.54	0.61	0.66
Ni (Ni@surface)-ρ_{th}=0.012	0.48	0.52	0.57	0.59	0.62	0.66	0.68
Ni (Ni@subsurface)	0.50	0.50	0.49	0.51	0.54	0.61	0.66
Ni (Ni@middle)	0.48	0.48	0.49	0.50	0.54	0.61	0.66
Ni (Ni@surface)-ρ_{th}=0.015	0.46	0.51	0.56	0.58	0.62	0.66	0.68
Ni (Ni@subsurface)	0.49	0.49	0.49	0.51	0.54	0.61	0.66
Ni (Ni@middle)	0.48	0.48	0.49	0.50	0.54	0.61	0.66
Ni (Ni@surface)-ρ_{th}=0.02	0.44	0.48	0.54	0.57	0.60	0.66	0.68
Ni (Ni@subsurface)	0.47	0.49	0.49	0.51	0.54	0.61	0.66
Ni (Ni@middle)	0.48	0.48	0.49	0.50	0.54	0.61	0.66
Ni (Ni@surface)-ρ_{th}=0.03	0.41	0.45	0.51	0.54	0.58	0.64	0.68
Ni (Ni@subsurface)	0.47	0.48	0.48	0.50	0.54	0.60	0.65
Ni (Ni@middle)	0.47	0.47	0.48	0.50	0.54	0.60	0.66
Ni-full coverage (Ni@surface)-ρ_{th}=0.004	0.62	0.63	0.58	0.58	0.58	0.62	0.65
Ni-full coverage (Ni@subsurface)	0.52	0.50	0.49	0.51	0.54	0.61	0.66
Ni-full coverage (Ni@middle)	0.49	0.49	0.49	0.51	0.55	0.61	0.66
Ni-full coverage (Ni@surface)-ρ_{th}=0.01	0.56	0.58	0.57	0.57	0.58	0.62	0.65
Ni-full coverage (Ni@subsurface)	0.51	0.49	0.49	0.51	0.54	0.61	0.66
Ni-full coverage (Ni@middle)	0.49	0.49	0.49	0.51	0.54	0.61	0.66
Ni-full coverage (Ni@surface)-ρ_{th}=0.012	0.55	0.57	0.57	0.56	0.58	0.62	0.65
Ni-full coverage (Ni@subsurface)	0.51	0.49	0.49	0.51	0.54	0.61	0.66
Ni-full coverage (Ni@middle)	0.49	0.49	0.49	0.51	0.54	0.61	0.66
Ni-full coverage (Ni@surface)-ρ_{th}=0.015	0.53	0.56	0.56	0.56	0.58	0.62	0.65
Ni-full coverage (Ni@subsurface)	0.50	0.49	0.49	0.50	0.54	0.61	0.66
Ni-full coverage (Ni@middle)	0.49	0.49	0.49	0.51	0.55	0.61	0.66
Ni-full coverage (Ni@surface)-ρ_{th}=0.02	0.51	0.54	0.56	0.56	0.58	0.62	0.65
Ni-full coverage (Ni@subsurface)	0.50	0.49	0.49	0.51	0.54	0.61	0.66
Ni-full coverage (Ni@middle)	0.49	0.49	0.49	0.51	0.55	0.61	0.66
Ni-full coverage (Ni@surface)-ρ_{th}=0.03	0.48	0.52	0.53	0.54	0.57	0.61	0.65
Ni-full coverage (Ni@subsurface)	0.49	0.48	0.48	0.50	0.54	0.61	0.66
Ni-full coverage (Ni@middle)	0.48	0.48	0.49	0.50	0.54	0.61	0.66

TABLE 6.5: The $\tilde{g}$ for plane Fe(001) surfaces as well as Fe(001) with different oxygen coverage for different σ and different ρ_{th} , the results for Fe and FeO are added to the table only for comparison

solid	σ=3.78	σ=2.78	σ=1.78	$\sigma = 1.53$	σ=1.28	σ=1.03	σ=0.78
Fe	1.37	1.37	1.43	1.56	1.85	2.41	3.25
FeO	1.73	1.73	1.83	1.97	2.28	2.73	3.43
Fe (Fe@surface)-ρ_{th}=0.0007	1.38	1.43	1.61	1.78	2.09	2.63	3.38
Fe (Fe@subsurface)	1.41	1.42	1.47	1.59	1.87	2.42	3.23
Fe (Fe@middle)	1.38	1.38	1.44	1.56	1.85	2.41	3.25
Fe (Fe@surface)-ρ_{th}=0.002	1.37	1.42	1.61	1.77	2.09	2.63	3.37
Fe (Fe@subsurface)	1.40	1.42	1.47	1.59	1.87	2.42	3.23
Fe (Fe@middle)	1.38	1.38	1.44	1.56	1.85	2.41	3.24
Fe (Fe@surface)-ρ_{th}=0.01	1.35	1.40	1.59	1.77	2.09	2.62	3.38
Fe (Fe@subsurface)	1.39	1.42	1.47	1.59	1.87	2.42	3.24
Fe (Fe@middle)	1.38	1.38	1.44	1.56	1.85	2.41	3.25
Fe (Fe@surface)-ρ_{th}=0.015	1.34	1.40	1.59	1.76	2.08	2.62	3.38
Fe (Fe@subsurface)	1.39	1.42	1.47	1.59	1.87	2.42	3.24
Fe (Fe@middle)	1.38	1.38	1.44	1.56	1.85	2.41	3.25
Fe-full coverage (Fe@surface)-ρ_{th}=0.002	1.58	1.66	1.81	1.94	2.19	2.66	3.38
Fe-full coverage (Fe@subsurface)	1.51	1.49	1.50	1.62	1.90	2.44	3.25
Fe-full coverage (Fe@middle)	1.39	1.39	1.45	1.57	1.85	2.40	3.24
Fe-full coverage (Fe@surface)-ρ_{th}=0.015	1.51	1.60	1.77	1.91	2.18	2.66	3.38
Fe-full coverage (Fe@subsurface)	1.48	1.48	1.50	1.62	1.90	2.44	3.25
Fe-full coverage (Fe@middle)	1.39	1.39	1.45	1.57	1.85	2.40	3.24
Fe-full coverage(2) (Fe@surface)-ρ_{th}=0.002	1.60	1.67	1.82	1.94	2.21	2.68	3.39
Fe-full coverage(2) (Fe@subsurface)	1.54	1.53	1.56	1.68	1.96	2.50	3.30
Fe-full coverage(2) (Fe@middle)	1.44	1.41	1.46	1.58	1.86	2.42	3.24
Fe-full coverage(2) (Fe@surface)-ρ_{th}=0.015	1.54	1.61	1.78	1.92	2.19	1.67	3.38
Fe-full coverage(2) (Fe@subsurface)	1.52	1.52	1.56	1.68	1.97	2.50	3.30
Fe-full coverage(2) (Fe@middle)	1.44	1.41	1.46	1.58	1.87	2.42	3.24
Fe-half coverage (Fe@surface)-ρ_{th}=0.015	1.48	1.55	1.71	1.85	2.13	2.63	3.35
Fe-half coverage (Fe@subsurface(near O))	1.46	1.47	1.51	1.62	1.90	2.43	3.24
Fe-half coverage (Fe@subsurface(far O))	1.46	1.46	1.48	1.60	1.88	2.44	3.24
Fe-half coverage (Fe@middle)	1.39	1.39	1.45	1.57	1.85	2.61	3.23
Fe-1/9 coverage(Fe@surface(nearO))-ρ_{th}=0.002	1.41	1.48	1.66	1.81	2.10	2.61	3.35
Fe-1/9 coverage(Fe@surface(farO))	1.38	1.42	1.61	1.78	2.09	2.62	3.36
Fe-1/9 coverage(Fe@sublayer(nearO))	1.44	1.46	1.50	1.61	1.88	2.42	3.24
Fe-1/9 coverage(Fe@sublayer(farO))	1.41	1.42	1.47	1.59	1.87	2.42	3.24
Fe-1/9 coverage(Fe@middle)	1.38	1.38	1.44	1.61	1.85	2.40	3.24
Fe-1/9 coverage(Fe@surface(nearO))-ρ_{th}=0.015	1.38	1.45	1.63	1.79	2.09	2.61	3.35
Fe-1/9 coverage(Fe@surface(farO))	1.35	1.40	1.59	1.62	2.08	2.62	3.36
Fe-1/9 coverage(Fe@sublayer(nearO))	1.42	1.46	1.50	1.61	1.88	2.42	3.24
Fe-1/9 coverage(Fe@sublayer(farO))	1.40	1.42	1.47	1.59	1.87	2.42	3.24
Fe-1/9 coverage(Fe@middle)	1.42	1.38	1.44	1.56	1.85	2.40	3.24

TABLE 6.6: The $\tilde{s}$ for plane Fe(001) surfaces as well as Fe(001) with different oxygen coverage for different σ and different ρ_{th} , the results for Fe and FeO are added to the table only for comparison

solid	σ=3.78	σ=2.78	σ=1.78	$\sigma = 1.53$	σ=1.28	σ=1.03	σ=0.78
Fe	0.47	0.47	0.48	0.50	0.53	0.59	0.62
FeO	0.64	0.64	0.65	0.67	0.68	0.70	0.66
Fe (Fe@surface)-original	1.25	0.88	0.67	0.65	0.65	0.67	0.67
Fe (Fe@sublayer)-original	0.70	0.55	0.50	0.51	0.54	0.59	0.62
Fe (Fe@middle)-original	0.47	0.47	0.48	0.49	0.53	0.59	0.62
Fe (Fe@surface)-ρ_{th}=0.004	0.53	0.58	0.61	0.63	0.64	0.66	0.65
Fe (Fe@sublayer)	0.52	0.52	0.50	0.51	0.54	0.59	0.62
Fe (Fe@middle)	0.47	0.47	0.48	0.49	0.53	0.59	0.62
Fe (Fe@surface)-ρ_{th}=0.007	0.48	0.53	0.59	0.61	0.63	0.66	0.65
Fe (Fe@sublayer))	0.50	0.51	0.50	0.51	0.54	0.59	0.62
Fe (Fe@middle)	0.47	0.47	0.48	0.49	0.53	0.59	0.62
Fe (Fe@surface)-ρ_{th}=0.01	0.46	0.50	0.57	0.59	0.63	0.66	0.65
Fe (Fe@sublayer)	0.49	0.50	0.50	0.51	0.54	0.59	0.62
Fe (Fe@middle)	0.47	0.47	0.48	0.49	0.53	0.59	0.62
Fe (Fe@surface)-ρ_{th}=0.015	0.43	0.47	0.54	0.57	0.61	0.65	0.65
Fe (Fe@sublayer)	0.47	0.49	0.50	0.51	0.54	0.60	0.62
Fe (Fe@middle)	0.47	0.47	0.48	0.49	0.53	0.60	0.62
Fe (Fe@surface)-ρ_{th}=0.03	0.37	0.40	0.48	0.51	0.57	0.62	0.64
Fe (Fe@sublayer)	0.44	0.46	0.48	0.50	0.53	0.59	0.62
Fe (Fe@middle)	0.47	0.46	0.47	0.49	0.52	0.58	0.62
Fe-full coverage (Fe@surface)-ρ_{th}=0.015	0.49	0.55	0.60	0.62	0.64	0.66	0.65
Fe-full coverage (Fe@sublayer)	0.51	0.51	0.51	0.52	0.55	0.60	0.62
Fe-full coverage (Fe@middle)	0.47	0.47	0.48	0.49	0.53	0.58	0.62
Fe-full coverage(2) (Fe@surface)-ρ_{th}=0.004	0.62	0.66	0.67	0.67	0.67	0.68	0.65
Fe-full coverage(2) (Fe@sublayer)	0.56	0.55	0.53	0.55	0.58	0.62	0.63
Fe-full coverage(2) (Fe@middle)	0.50	0.49	0.50	0.50	0.54	0.59	0.62
Fe-full coverage(2) (Fe@surface)-ρ_{th}=0.01	0.54	0.59	0.63	0.64	0.66	0.68	0.65
Fe-full coverage(2) (Fe@sublayer)	0.54	0.54	0.53	0.55	0.58	0.62	0.63
Fe-full coverage(2) (Fe@middle)	0.49	0.49	0.49	0.51	0.54	0.59	0.62
Fe-full coverage(2) (Fe@surface-ρ_{th}=0.015	0.51	0.56	0.61	0.63	0.65	0.67	0.65
Fe-full coverage(2) (Fe@sublayer)	0.53	0.53	0.53	0.55	0.58	0.62	0.64
Fe-full coverage(2) (Fe@middle)	0.50	0.49	0.49	0.51	0.54	0.59	0.62
Fe-full coverage(2) (Fe@surface-ρ_{th}=0.02	0.49	0.54	0.59	0.61	0.64	0.66	0.65
Fe-full coverage(2) (Fe@sublayer)	0.52	0.53	0.53	0.54	0.57	0.62	0.63
Fe-full coverage(2) (Fe@middle)	0.49	0.49	0.49	0.50	0.54	0.59	0.62
Fe-half coverage (Fe@surface) (ρ_{th}=0.015)	0.47	0.52	0.58	0.60	0.63	0.66	0.65
Fe-half coverage (Fe@subsurface(near O))	0.49	0.50	0.50	0.51	0.54	0.59	0.62
Fe-half coverage (Fe@subsurface(far O))	0.49	0.50	0.50	0.51	0.55	0.60	0.62
Fe-half coverage (Fe@middle)	0.47	0.47	0.47	0.49	0.52	0.58	0.62
Fe-1/9 coverage(Fe@surface(nearO))-original	1.44	0.95	0.70	0.67	0.66	0.67	0.65
Fe-1/9 coverage(Fe@surface(farO))-original	1.36	0.89	0.67	0.65	0.65	0.67	0.65
Fe-1/9 coverage(Fe@sublayer(nearO))-original	0.71	0.55	0.50	0.51	0.60	0.59	0.62
Fe-1/9 coverage(Fe@sublayer(farO))-original	0.74	0.56	0.50	0.51	0.54	0.59	0.62
Fe-1/9 coverage(Fe@middle)-original	0.47	0.47	0.48	0.49	0.53	0.59	0.62
Fe-1/9 coverage(Fe@surface(nearO)-$\rho_{\text{th}} = 0.004$	0.55	0.60	0.63	0.64	0.65	0.67	0.65
Fe-1/9 coverage(Fe@surface(farO))	0.54	0.58	0.61	0.62	0.64	0.66	0.65
Fe-1/9 coverage(Fe@sublayer(nearO))	0.53	0.52	0.50	0.51	0.54	0.60	0.62
Fe-1/9 coverage(Fe@sublayer(farO))	0.52	0.52	0.50	0.51	0.54	0.58	0.62
Fe-1/9 coverage(Fe@middle)	0.47	0.47	0.48	0.49	0.53	0.59	0.62
Fe-1/9 coverage(Fe@surface(nearO)-$\rho_{\text{th}} = 0.012$	0.46	0.51	0.57	0.60	0.62	0.66	0.65
Fe-1/9 coverage(Fe@surface(farO))	0.45	0.49	0.56	0.58	0.62	0.66	0.64
Fe-1/9 coverage(Fe@sublayer(nearO))	0.49	0.50	0.50	0.51	0.54	0.59	0.62
Fe-1/9 coverage(Fe@sublayer(farO))	0.48	0.50	0.50	0.51	0.54	0.59	0.62
Fe-1/9 coverage(Fe@middle)	0.47	0.47	0.48	0.49	0.53	0.58	0.62
Fe-1/9 coverage(Fe@surface(nearO))-$\rho_{\text{th}} = 0.015$	0.44	0.49	0.56	0.58	0.62	0.65	0.65
Fe-1/9 coverage(Fe@surface(farO))	0.43	0.47	0.54	0.57	0.61	0.65	0.64
Fe-1/9 coverage(Fe@sublayer(nearO))	0.48	0.50	0.50	0.51	0.54	0.59	0.62
Fe-1/9 coverage(Fe@sublayer(farO))	0.47	0.49	0.50	0.51	0.54	0.59	0.62
Fe-1/9 coverage(Fe@middle)	0.47	0.47	0.48	0.49	0.53	0.59	0.62
Fe-1/9 coverage(Fe@surface(nearO))-$\rho_{\text{th}} = 0.02$	0.42	0.47	0.54	0.56	0.61	0.65	0.64
Fe-1/9 coverage(Fe@surface(farO))	0.41	0.45	0.52	0.55	0.60	0.64	0.64
Fe-1/9 coverage(Fe@sublayer(nearO))	0.48	0.49	0.50	0.51	0.54	0.60	0.62
Fe-1/9 coverage(Fe@sublayer(farO))	0.46	0.48	0.49	0.51	0.54	0.60	0.62
Fe-1/9 coverage(Fe@middle)	0.47	0.47	0.48	0.49	0.53	0.59	0.62
Fe-1/9 coverage(Fe@surface(nearO))-$\rho_{\text{th}} = 0.03$	0.38	0.43	0.50	0.53	0.58	0.63	0.64
Fe-1/9 coverage(Fe@surface(farO))	0.37	0.41	0.48	0.51	0.57	0.62	0.64
Fe-1/9 coverage(Fe@sublayer(nearO))	0.46	0.48	0.49	0.50	0.53	0.59	0.62
Fe-1/9 coverage(Fe@sublayer(farO))	0.44	0.46	0.48	0.50	0.53	0.59	0.62
Fe-1/9 coverage(Fe@middle)	0.47	0.47	0.47	0.49	0.52	0.58	0.62

Bibliography

[1] E. Schrödinger. *Phys. Rev.*, 28(6):1049–1070, 1926.

[2] R. Oppenheimer M. Born. *Ann. Phys.*, 389:457, 1927.

[3] D. R. Hartree. *Proc. Cambridge Philos. Soc.*, 24:89, 1928.

[4] D. R. Hartree. *Proc. Cambridge Philos. Soc.*, 24:111, 1928.

[5] D. R. Hartree. *Proc. Cambridge Philos. Soc.*, 24:426, 1928.

[6] V. Fock. *Z. Phys.*, 61:126, 1930.

[7] V. Fock. *Z. Phys.*, 62:795, 1930.

[8] J. C. Slater. *Phys. Rev.*, 35:210, 1930.

[9] J. C. Slater. *Phys. Rev.*, 81:385, 1951.

[10] P. Hohenberg and W. Kohn. *Phys. Rev.*, 136:B864, 1964.

[11] L. H. Thomas. *Proc. Cambridge Philos. Soc.*, 23:542, 1927.

[12] E. Fermi. *Rend. Accad. Naz. Lincei*, 6:602, 1927.

[13] P. A. M. Dirac. *Proc. Cambridge Philos. Soc.*, 26:376, 1930.

[14] W. Kohn and L. J. Sham. *Phys. Rev.*, 140:A1133, 1965.

[15] J. P. Perdew and K. Schmidt. *AIP Conf. Proc.*, 577:1, 2001.

[16] W. A. Curtin and N. W. Ashcroft. *Phys. Rev. A*, 32:2909–2919, Nov 1985.

[17] Stefan Grimme. *J. Comput. Chem.*, 25:1463, 2004.

[18] Stefan Grimme. *J. Comput. Chem.*, 27:1787, 2006.

[19] Stefan Grimme, Jens Antony, Stephan Ehrlich, and Helge Krieg. *J. Chem. Phys.*, 132:
154104, 2010.

[20] S. Grimme, S. Ehrlich, and L. Goerigk. *J. Comput. Chem.*, 32:1456, 2011.

[21] M. Dion, H. Rydberg, E. Schröder, D. C. Langreth, and B. I. Lundqvist. *Phys. Rev.
Lett.*, 92:246401, 2004. **95**, 109902(E) (2005).

[22] R.G. Parr and W. Yang. *Density-Functional Theory of Atoms and Molecules*. Oxford
University Press, USA, 1994.

[23] D. M. Ceperley and B. J. Alder. *Phys. Rev. Lett.*, 45:566–569, 1980.

[24] J. P. Perdew and Y Wang. *Phys. Rev. B*, 45:13244, 1992.

[25] S. H. Vosko, L. Wilk, and M. Nusair. *Can. J. Phys.*, 58:1200, 1980.

[26] M. Ropo, K. Kokko, and L. Vitos. *Phys. Rev. B*, 77:195445, 2008.

[27] J.P. Perdew D.C. Langreth. *Solid State Commun.*, 31:567–571, 1979.

[28] J. P. Perdew, K. Burke, and M. Ernzerhof. *Phys. Rev. Lett.*, 77:3865, 1996. **78**,
1396(E) (1997).

[29] A. D. Becke. *Phys. Rev. A*, 38:3098, 1988.

[30] J. P. Perdew, A. Ruzsinszky, G. I. Csonka, O. A. Vydrov, G. E. Scuseria, L. A. Con-
stantin, X. Zhou, and K. Burke. *Phys. Rev. Lett.*, 100:136406, 2008. **102**, 039902(E)
(2008).

[31] A. D. Becke. *J. Chem. Phys.*, 98:1372, 1993.

[32] P. J. Stephens, F. J. Devlin, C. F. Chabalowski, and M. J. Frisch. *J. Phys. Chem.*,
98:11623, 1994.

[33] E. H. Lieb and S. Oxford. *Int. J. Quantum Chem.*, 19:427, 1981.

[34] F. Tran, R. Laskowski, P. Blaha, and K. Schwarz. *Phys. Rev. B*, 75:115131, 2007.

[35] P. Haas, F. Tran, and P. Blaha. *Phys. Rev. B*, 79:085104, 2009. **79**, 209902(E) (2009).

[36] J. Tao, J. P. Perdew, V. N. Staroverov, and G. E. Scuseria. *Phys. Rev. Lett.*, 91: 146401, 2003.

[37] J. P. Perdew, L.A. Constantin, E. Sagvolden, and K. Burke. *Phys. Rev. Lett*, 97: 223002, 2006.

[38] Y. Zhao and D. G. Truhlar. *J. Chem. Phys.*, 128:184109, 2008.

[39] A. Ruzsinszky, G. I. Csonka, and G. E. Scuseria. *J. Chem. Theory Comput.*, 5:763, 2009.

[40] G. I. Csonka, J. P. Perdew, A. Ruzsinszky, P. H. T. Philipsen, S. Lebègue, J. Paier, O. A. Vydrov, and J. Ángyán. *Phys. Rev. B*, 79:155107, 2009.

[41] J. Sun, B. Xiao, Y. Fang, R. Haunschild, P. Hao, A. Ruzsinszky, G. I. Csonka, G. E. Scuseria, and J. P. Perdew. *Phys. Rev. Lett.*, 111:106401, 2013.

[42] A. D. Becke and K. E. Edgecombe. *J. Chem. Phys.*, 92:5397, 1990.

[43] J. Sun, A. Ruzsinszky, and J. P. Perdew. *Phys. Rev. Lett.*, 115:036402, 2015.

[44] J. P. Perdew, A. Ruzsinszky, G. I. Csonka, L. A. Constantin, and J. Sun. *Phys. Rev. Lett.*, 103:026403, 2009. **106**, 179902 (2011).

[45] M. Ernzerhof and G. E. Scuseria. *J. Chem. Phys.*, 110:5029, 1999.

[46] C. Adamo and V. Barone. *J. Chem. Phys.*, 110:6158, 1999.

[47] J. Heyd, G. E. Scuseria, and M. Ernzerhof. *J. Chem. Phys.*, 118:8207, 2003. **124**, 219906 (2006).

[48] A. V. Krukau, O. A. Vydrov, A. F. Izmaylov, and G. E. Scuseria. *J. Chem. Phys.*, 125:224106, 2006.

[49] Hideki YUKAWA. *Proceedings of the Physico-Mathematical Society of Japan. 3rd Series*, 17:48–57, 1935.

[50] Fabien Tran and Peter Blaha. *Phys. Rev. B*, 83:235118, 2011.

[51] David Bohm and David Pines. *Physical Review*, 82(5):625, 1951.

[52] David Pines and David Bohm. *Physical Review*, 85(2):338, 1952.

[53] David Bohm and David Pines. *Physical Review*, 92(3):609, 1953.

[54] D. C. Langreth and J. P. Perdew. *Solid State Commun.*, 17:1425, 1975.

[55] D. C. Langreth and J. P. Perdew. *Phys. Rev. B*, 15:2884, 1977.

[56] E. Runge and E. K. U. Gross. *Phys. Rev. Lett.*, 52:997–1000, 1984.

[57] E. K. U. Gross and Walter Kohn. *Phys. Rev. Lett.*, 55:2850–2852, 1985.

[58] J. Harl and G. Kresse. *Phys. Rev. B*, 77:045136, 2008.

[59] K. Terakura, T. Oguchi, A. R. Williams, and J. Kübler. *Phys. Rev. B*, 30:4734, 1984.

[60] G. A. Sawatzky and J. W. Allen. *Phys. Rev. Lett.*, 53:2339, 1984.

[61] W. Metzner and D. Vollhardt. *Phys. Rev. Lett.*, 62:324, 1989.

[62] E. Muller-Hartmann. *Z. Phys. B Condens. Matter*, 74:507, 1989.

[63] U. Brandt and C. Mielsch. *Z. Phys. B Condens. Matter*, 75:365, 1989.

[64] V. Janis. *Z. Phys. B Condens. Matter*, 83:227, 1991.

[65] W. Yang, Y. Zhang, and P. W. Ayers. *Phys. Rev. Lett.*, 84:5172, 2000.

[66] R. Requist and O. Pankratov. *Phys. Rev. B.*, 77:235121, 2008.

[67] Peitao Liu, Cesare Franchini, Martijn Marsman, and Georg Kresse. *J. Phys. Condens. Matter*, 32(1):015502, oct 2019.

[68] V. I. Anisimov, F. Aryasetiwan, and A. I. Lichtenstein. *J. Phys. Condens. Matter*, 9: 767, 1997.

[69] S. L. Dudarev and S. Y. Humphreys C. J. Sutton A. P. Botton, G. A. Savrasov. *J. Phys. Rev. B*, 57:1505, 1998.

[70] J. Hubbard. *Proc. R. Soc. London A*, 276:238, 1963.

[71] J. Hubbard. *Proc. R. Soc. London A*, 277:237, 1964.

[72] J. Hubbard. *Proc. R. Soc. London A*, 281:401, 1964.

[73] J. Hubbard. *Proc. R. Soc. London A*, 285:542, 1965.

[74] J. Hubbard. *Proc. R. Soc. London A*, 296:82, 1967.

[75] J. Hubbard. *Proc. R. Soc. London A*, 296:100, 1967.

[76] V. I. Anisimov, J. Zaanen, and O. K. Andersen. *Phys. Rev. B*, 44:943, 1991.

[77] M. T. Czyżyk and G. A. Sawatzky. *Phys. Rev. B*, 49:14211, 1994.

[78] A. G. Petukhov, I. I. Mazin, L. Chioncel, and A. I. Lichtenstein. Correlated metals and the LDA + u method. *Phys. Rev. B*, 67:153106, 2003.

[79] V. I. Anisimov, A. V. Kozhevnikov, M. A. Korotin, A. V. Lukoyanov, and D. A. Khafizullin. *J. Phys. Condens. Matter*, 19:106206, 2007.

[80] V. I. Anisimov, I. V. Solovyev, M. A. Korotin, M. T. Czyżyk, and G. A. Sawatzky. *Phys. Rev. B*, 48:16929, 1993.

[81] A. I. Lichtenstein and J Anisimov, V. I. Zaanen. *J. Phys. Rev. B*, 52:R5467, 1995.

[82] C. Di Valentin, G. Pacchioni, and A. Selloni. *J. Phys. Chem. C*, 113:20543, 2009.

[83] A. I. Liechtenstein, V. I. Anisimov, and J. Zaanen. *Phys. Rev. B*, 52:R5467, 1995.

[84] A Messiah. Quantenmechanik volume ii, 1979.

[85] John C Slater. Quantum theory of atomic structure. Technical report, 1960.

[86] L. Vaguier, H. Jiang, and S. Biermann. *Phys. Rev. B.*, 86:165105, 2012.

[87] E. Bousquet and N. Spaldin. *Phys. Rev. B*, 82:220402, 2010.

[88] T. Jeong and W. E. Pickett. *J. Phys. Condens. Matter*, 18:6289, 2006.

[89] L. dé Medici. *Phys. Rev. B.*, 83:205112, 2011.

[90] L. dé Medici, J. Mravije, and A. Georges. *Phys. Rev. Lett.*, 107:256401, 2011.

[91] F. Bultmark, F. Cricchio, O. Grånäs, and L. Nordström. *Phys. Rev. B*, 80:035121, 2009.

[92] P. H. Dederichs, S. Blügel, R. Zeller, and H. Akai. *Phys. Rev. Lett.*, 53.

[93] M. S. Hybertsen, M. Schlüter, and N. E. Christensen. *Phys. Rev. B*, 39:9028–9041, 1989.

[94] G. K. H. Madsen and P. Novák. *Europhys. Lett.*, 69:777, 2005.

[95] M. Springer and F. Aryasetiawan. *Phys. Rev. B*, 57:4364–4368, 1998.

[96] F. Aryasetiawan, M. Imada, A. Georges, G. Kotliar, S. Biermann, and A. I. Lichtenstein. *Phys. Rev. B*, 70:195104, 2004.

[97] F. Aryasetiawan, K. Karlsson, O. Jepsen, and U. Schönberger. *Phys. Rev. B*, 74: 125106, 2006.

[98] Ersoy Şaşıoğlu, Christoph Friedrich, and Stefan Blügel. *Phys. Rev. Lett.*, 109:146401, Oct 2012.

[99] M. Cococcioni and S. de Gironcoli. *Phys. Rev. B*, 71:035105, 2005.

[100] W. E. Pickett, S. C. Erwin, and E. C. Ethridge. *Phys. Rev. B*, 58:1201–1209, 1998.

[101] Leila Kalantari, Fabien Tran, and Peter Blaha. *Phys. Rev. B*, 104:155127, 2021.

[102] Fabien Tran and Peter Blaha. *Phys. Rev. Lett.*, 102:226401, 2009.

[103] F. Tran, J. Doumont, L. Kalantari, A. W. Huran, M. A. L. Marques, and P. Blaha. *J. Appl. Phys.*, 126:110902, 2019.

[104] M. A. L. Marques, J. Vidal, M. J. T. Oliveira, L. Reining, and S. Botti. *Phys. Rev. B*, 83:035119, 2011.

[105] T. Rauch, M. A. L. Marques, and S. Botti. *J. Chem. Theory Comput.*, 16:2654, 2020.

[106] T. Rauch, M. A. L. Marques, and S. Botti. *Phys. Rev. B*, 101:245163, 2020. **102**, 119902(E) (2020).

[107] L. Hedin. *Phys. Rev.*, 139:A796–A823, 1965.

[108] Abhilash Patra, Subrata Jana, Prasanjit Samal, Fabien Tran, Leila Kalantari, Jan Doumont, and Peter Blaha. *J. Phys. Chem. C*, 125(20):11206–11215, 2021.

[109] M. Kuisma, J. Ojanen, J. Enkovaara, and T. T. Rantala. *Phys. Rev. B*, 82:115106, 2010.

[110] Bimal Neupane, Hong Tang, Niraj K. Nepal, Santosh Adhikari, and Adrienn Ruzsinszky. *Phys. Rev. Materials*, 5:063803, Jun 2021.

[111] Thilo Aschebrock and Stephan Kümmel. *Phys. Rev. Research*, 1:033082, 2019.

[112] P. Blaha, K. Schwarz, G. K. H. Madsen, D. Kvasnicka, J. Luitz, R. Laskowski, F. Tran, and L. D. Marks. *WIEN2k: An Augmented Plane Wave plus Local Orbitals Program for Calculating Crystal Properties*. Vienna University of Technology, Austria, 2018.

[113] P. Blaha, K. Schwarz, F. Tran, R. Laskowski, G. K. H. Madsen, and L. D. Marks. *J. Chem. Phys.*, 152:074101, 2020.

[114] D. J. Singh and L. Nordström. *Planewaves, Pseudopotentials and the LAPW Method, 2nd ed.* Springer, Berlin, 2006.

[115] E. Sjöstedt, L. Nordström, and D. J. Singh. *Solid State Commun.*, 114:15, 2000.

[116] G. K. H. Madsen, P. Blaha, K. Schwarz, E. Sjöstedt, and L. Nordström. *Phys. Rev. B*, 64:195134, 2001.

[117] John P. Perdew and Yue Wang. *Phys. Rev. B*, 98:079904, 2018.

[118] J. P. Perdew, J. A. Chevary, S. H. Vosko, K. A. Jackson, M. R. Pederson, D. J. Singh, and C. Fiolhais. *Phys. Rev. B*, 46:6671, 1992. **48**, 4978(E) (1993).

[119] J. P. Perdew, M. Ernzerhof, and K. Burke. *J. Chem. Phys.*, 105:9982, 1996.

[120] Z. Wu and R. E. Cohen. *Phys. Rev. B*, 73:235116, 2006. Y. Zhao and D. G. Truhlar, *ibid.* **78**, 197101 (2008); Z. Wu and R. E. Cohen, *ibid.* **78**, 197102 (2008).

[121] A. D. Becke. *J. Chem. Phys.*, 98:5648, 1993.

[122] M. A. L. Marques, M. J. T. Oliveira, and T. Burnus. *Comput. Phys. Commun.*, 183:2272, 2012.

[123] S. Lehtola, C. Steigemann, M. J. T. Oliveira, and M. A. L. Marques. *SoftwareX*, 7:1, 2018.

[124] J. Klimeš and A. Michaelides. *J. Chem. Phys.*, 137:120901, 2012.

[125] Yan Zhao and Donald G. Truhlar. *J. Chem. Theory Comput.*, 3:289, 2007.

[126] O. A. von Lilienfeld, I. Tavernelli, U. Rothlisberger, and D. Sebastiani. *Phys. Rev. Lett.*, 93:153004, 2004.

[127] Y. Y. Sun, Y. Kim, K. Lee, and S. B. Zhang. *J. Chem. Phys.*, 129:154102, 2008.

[128] E. Tapavicza, I. Lin, von O. A. von Lilienfeld, I. Tavernelli, M. D. Coutinho Neto, and U. Rothlisberger. *J. Chem. Theory Comput.*, 3:1673, 2007.

[129] Qin Wu and Weitao Yang. *J. Chem. Phys.*, 116:515, 2002.

[130] A. D. Becke and E. R. Johnson. *J. Chem. Phys.*, 127:154108, 2007.

[131] Alexandre Tkatchenko and Matthias Scheffler. *Phys. Rev. Lett.*, 102:073005, 2009.

[132] A. Tkatchenko, R. A. DiStasio, Jr., R. Car, and M. Scheffler. *Phys. Rev. Lett.*, 108: 236402, 2012.

[133] D. G. A. Smith, L. A. Burns, K. Patkowski, and C. D. Sherrill. *J. Phys. Chem. Lett.*, 7:2197–2203, 2016.

[134] H. Casimir and D. Polder. *Phys. Rev.*, 73:360, 1948.

[135] A. O. von Lilienfeld and A. Tkatchenko. *J. Chem. Phys.*, 132:234109, 2010.

[136] Y. Muto. *J. Phys. Math. Soc. Jpn*, 17:629, 1943.

[137] Axilrod B. M. and E. Teller. *J. Chem. Phys.*, 11:299, 1943.

[138] X. Chu and A. Dalgarno. *Phys. Chem. Chem. Phys.*, 121:4083, 2004.

[139] K. T. Tang. *Phys. Rev.*, 177:108, 1969.

[140] A. D. Becke. *J. Chem. Phys.*, 98:5648, 1993.

[141] S. Grimme, A. Hansen, J. G. Brandenburg, and C. Bannwarth. *Chem. Rev.*, 116:5105, 2016.

[142] Y. Zhang and W. Yang. *Phys. Rev. Lett.*, 80:890, 1998.

[143] G. Román-Pérez and J. M. Soler. *Phys. Rev. Lett.*, 103:096102, 2009.

[144] F. Tran, L. Kalantari, B. Traoré, X. Rocquefelte, and P. Blaha. *Phys. Rev. Materials*, 3:063602, 2019.

[145] Oleg A. Vydrov and Troy Van Voorhis. *Phys. Rev. Lett.*, 103:063004, 2009.

[146] Oleg A. Vydrov and Troy Van Voorhis. *J. Chem. Phys.*, 133:244103, 2010.

[147] R. Sabatini, T. Gorni, and S. de Gironcoli. *Phys. Rev. B*, 87:041108(R), 2013.

[148] Aleksandr V. Terentjev, Lucian A. Constantin, and J. M. Pitarke. *Phys. Rev. B*, 98: 214108, 2018.

[149] J. Harl, L. Schimka, and G. Kresse. *Phys. Rev. B*, 81:115126, 2010.

[150] S. Lebègue, J. Harl, Tim Gould, J. G. Ángyán, G. Kresse, and J. F. Dobson. *Phys. Rev. Lett.*, 105:196401, 2010.

[151] J. F. Dobson, A. White, and A. Rubio. *Phys. Rev. Lett.*, 96:073201, 2006.

[152] Tobias Schaefer and Georg Kresse. Low-Scaling MP2 for Solids. In *APS March Meeting Abstracts*, volume 2018 of *APS Meeting Abstracts*, page P18.001, January 2018.

[153] J. Heyd, J. E. Peralta, G. E. Scuseria, and R. L. Martin. *J. Chem. Phys.*, 123:174101, 2005.

[154] E. R. Johnson and A. D. Becke. *J. Chem. Phys.*, 124:174104, 2006.

[155] R. T. Sharp and G. K. Horton. *Phys. Rev.*, 90:317, 1953.

[156] J. D. Talman and W. F. Shadwick. *Phys. Rev. A*, 14:36, 1976.

[157] A. D. Becke and M. R. Roussel. *Phys. Rev. A*, 39:3761, 1989.

[158] James D. Talman. *Comput. Phys. Commun.*, 54:85, 1989.

[159] K. D. Sen. *J. Chem. Phys.*, 116:9570, 2002.

[160] Fabien Tran, Peter Blaha, and Karlheinz Schwarz. *J. Phys.: Condens. Matter*, 19: 196208, 2007.

[161] Axel D. Becke and Erin R. Johnson. *J. Chem. Phys.*, 124:221101, 2006.

[162] David Koller, Fabien Tran, and Peter Blaha. *Phys. Rev. B*, 85:155109, 2012.

[163] Tomá š Rauch, Miguel A. L. Marques, and Silvana Botti. Erratum:[phys. rev. b 101, 245163 (2020)]. *Phys. Rev. B*, 102:119902, Sep 2020.

[164] Fabien Tran, Jan Doumont, Leila Kalantari, Peter Blaha, Tomáš Rauch, Pedro Borlido, Silvana Botti, Miguel A. L. Marques, Abhilash Patra, Subrata Jana, and Prasanjit Samal. *J. Chem. Phys.*, 155:104103, 2021.

Leila Kalantari

Arbessbachgasse 30/1/7
1190 Vienna
Austria
✆ +4367761833250
✉ leila74kalantari@mail.com

Education

2017-2021 **PhD, Theoretical Materials Chemistry**, TU Wien, Vienna, Austria.
- **Ph.D. Thesis:** "*Development, tests and application of DFT based methods specifically to lower dimensional systems*," under supervision of **Prof. Peter Blaha**

2008-2011 **M.Sc. in Physics**, University of Payame Noor, Tehran-Parand, Iran.
- **M.Sc. Thesis:** "*Study of Electronic structure of Graphene doped with Fluorine*," under supervision of **Dr. Amir Abbas Sabouri Dodaran**

1992-1996 **B.Sc. in Physics**, University of Gilan, Iran.

Experiences

2017-2021 **Project assistant**, TU Wien, Institute of Materials Chemistry, Vienna, Austria.

1996-2015 **Physics teacher and lab manager**, Isfahan, Iran.

1993-1995 **Tutor**, Classical Mechanics, Gilan, Iran.

Skills

- **Codes**
  WIEN2k, Quantum ESPRESSO
- **Computer languages**
  Python, Matlab, Fortran

Languages

- **English:** advanced
- **German:** B2
- **Persion:** mother tongue

Publications

- Computational Study of Y NMR Shielding in Intermetallic Yttrium Compounds, *Leila Kalantari, Khoong Hong Khoo, Robert Laskowski, Peter Blaha; The Journal of Physical Chemistry C 121 (51), 28454-28461 (2017)*
- Orbital-free approximations to the kinetic-energy density in exchange-correlation MGGA functionals: Tests on solids, *Fabien Tran, Péter Kovács, Leila Kalantari, Georg K. H. Madsen, Peter Blaha; The Journal of chemical physics 149 (14), 144105 (2018)*

○ Nonlocal van der Waals functionals for solids: Choosing an appropriate one *Fabien Tran, Leila Kalantari, Boubacar Traoré, Xavier Rocquefelte, Peter Blaha; Physical Review Materials 3 (6), 063602, (2019).*

○ Semilocal exchange-correlation potentials for solid-state calculations: Current status and future directions *F Tran, J Doumont, L Kalantari, AW Huran, MAL Marques, P Blaha; Journal of Applied Physics 126 (11), 110902, (2019)*

○ Efficient Band Structure Calculation of Two-Dimensional Materials from Semilocal Density Functionals, *A Patra, S Jana, P Samal, F Tran, L Kalantari, J Doumont, P Blaha; J. Phys. Chem. C 2021, 125, 20, 11206–11215, (2021)*

○ Band gap of two-dimensional materials: thorough assessment of modern exchange-correlation functionals *Fabien Tran, Jan Doumont, Leila Kalantari, Peter Blaha, Tomáš Rauch, Pedro Borlido, Silvana Botti, Miguel A. L. Marques, Abhilash Patra, Subrata Jana, Prasanjit Samal; J. Chem. Phys. 155, 104103 (2021)*

○ Elucidating the formation and active state of Cu co-catalysts for photocatalytic hydrogen evolution *Jasmin S. Schubert, Leila Kalantari, Andreas Lechner, Ariane Giesriegl, Sreejith P. Nandan, Pablo Alaya Leiva, Peter Blaha, Alexey Cherevan, Dominik Eder; J. Mater. Chem. A, 9(38), 21958-21971, (2021).*

○ Density analysis for estimating the degree of on-site correlation on transition-metal atoms in extended systems, *Leila Kalantari, Fabien Tran, Peter Blaha; Phys. Rev. B 104, 155127, (2021)*

○ Density functional theory study of metal and metal-oxide nucleation and growth on the anatase TiO_2(101) surface, *Leila Kalantari, Fabien Tran, Peter Blaha; submitted*

Reference

○ **Prof. Peter Blaha**
Institute of Material Chemistry
Vienna University of Technology
Getreidemarkt 9/165-TC
Tel.: +43-1-58801-165300
Fax: +43-1-58801-165982
Email: pblaha@theochem.tuwien.ac.at

Die approbierte gedruckte Originalversion dieser Dissertation ist an der TU Wien Bibliothek verfügbar.
The approved original version of this doctoral thesis is available in print at TU Wien Bibliothek.

TU **Bibliothek**
Your knowledge hub
WIEN